Creating a dynamic model of a gas turbine in the MVEM framework using an Ellipse compressor model

Edvin Hansson

Master of Science Thesis in Electrical Engineering

Creating a dynamic model of a gas turbine in the MVEM framework using an Ellipse compressor model:

Edvin Hansson

LiTH-ISY-EX-20/5285--SE

Supervisor: **Kristoffer Ekberg**
ISY, Linköpings universitet

Examiner: **Prof. Lars Eriksson**
ISY, Linköpings universitet

Division of Automatic Control
Department of Electrical Engineering
Linköping University
SE-581 83 Linköping, Sweden

Sammanfattning

I takt med att lagstiftningen skärps mer och mer på utsläppsområdet ställs större krav på gasturbiners miljöpåverkan. Tillverkare vill som följd av detta minimera utsläppen, men ändå bibehålla prestanda. För att uppnå detta krävs optimeringar av befintliga principer och i vissa fall helt nya tankar, lösningar och idéer. Ett led i att ta fram nya, bättre gasturbiner är att skapa prototyper och testköra dessa. Det är emellertid en kostsam process att konstruera och testköra en gasturbin, vilket gör vinsterna med pålitliga simuleringsmodeller påtagliga både tidsmässigt och ekonomiskt.

Detta arbete innefattar huvudsakligen konstruktionen av en dynamisk modell av en gasturbin. Den modellerade gasturbinen har nio kompressorsteg, en roterande axel samt ett turbinsteg. Modelleringen av kompressorn utgör en stor del av arbetet, där Ellipsemodellen introduceras och implementeras på gasturbinskompressorer. Ellipsemodellen parametriserar en inmatad kompressormapp med elliptiska ekvationer och möjliggör ett steg från den sedvanliga modelleringen av kompressorer som lookup-tables som annars är förhärskande i gasrtubin-modellering. Kompressorns nio steg skalas och modelleras individuellt med en inbördes skalningsprincip som bygger på de respektive stegens maximala tryck-kvot vid optimal hastighet. Den konstruerade kompressorn sätts i en simulerad testbänk och en kompressormapp skapas, vilken inses i mångt och mycket likna en allmän kompressormapp.

En detaljerad genomgång ges av alla gasturbinens submodeller av kompressor, förbränning och bränsleinsprutning samt turbin och rotationsdynamik. De viktigaste ekvationerna som styr respektive modell, samt inspirationskällor till dessa föredras under modelleringskapitlet. Vidare avhandlas simuleringsscenario och den använda programvaran Matlab Simulink beskrivs i korthet.

Den totala gasturbinmodellen testas i stationär drift och en längre transient genom dess föredragna arbetsområde. Resultaten därifrån utvärderas och en alternativ regulatorstruktur föreslås och implementeras. Resultaten med den alternativa regulatorstrukturen diskuteras och jämförs med de identifierade bristerna som skulle åtgärdas, och det konstateras att den nya regulatorn lyckas åtgärda de identifierade bristerna i den ursprungliga designen.

Abstract

The legislations on greenhouse gas emissions are getting tougher and tougher every year. This drives the demand for energy efficient gas turbines with as low emissions as possible. This poses the challenge to manufacturers of constructing gas turbines with lessened environmental impact, but with maintained performance. To obtain this, there is a need of optimization of current principles along with completely new ideas and solutions. One part of developing new, improved gas turbine configurations is to create prototypes and test them. However, creating and testing a gas turbine is a both expensive and time consuming. They are large in every sense of the word: they are long, heavy, demand lots of fuel, create massive air flows and generate a lot of energy. Designing, building and testing new turbine configurations are therefore risky, as it requires investing lots of time and money. This means that it is highly profitable to have accurate, dependable simulation models.

This thesis uses Matlab Simulink to create a dynamic model of a single axis gas turbine with nine stage compressor and a single stage turbine. The modeling of the compressor composes a large part of the work in the thesis, where the Ellipse compressor model is introduced and implemented on a gas turbine compressor. The Ellipse model creates a parametric model of each of the nine compressor stages by the use of elliptic equations. The goal is to provide an alternative to the look-up table model of compressors, which are common to find in modeling papers today. In the design of the compressor, a single stage map is scaled nine different ways to mimic the design of a real life nine stage compressor. The stage scaling principle is based on a linear model that correlates stage size with maximum available pressure ratio at optimal speed. The constructed compressor model is put in a simulated test bench and a compressor map is created. The map is found to in most aspects resemble a general compressor map.

Furthermore, the thesis contains a run-through of the sub-models of the rest of the turbine, namely combustion chamber and fuel injection, compressor turbine and torque dynamics. For each sub-model, the most important equations and inspirations for these are presented. Finally, a description of the simulation scenarios and the simulation software, Matlab Simulink, is provided.

The model is tested in steady-sate operation around its optimal operating point, as well as during a transient in a benign operating zone, in terms of efficiency. The results of these simulations are analyzed and a flaw in the control strategy is pinpointed. An alternate control strategy is proposed, described and implemented. A comparison is made between the original and alternative control strategies, and it is concluded that the new controller manages to mitigate the problems identified in the original simulations.

Acknowledgments

I would like to thank my family and friends, who have stayed by my side through-out the duration of this thesis. A special thanks to my loving and supporting girlfriend Lisa, who has kept me going and motivated me to keep on working. I would never have made it without you.

No small amount of gratitude goes to my brother in arms (or at least studies), Linus, who in the role as opponent has supported me and driven me on towards a finished thesis he could oppose.

Norrköping, march 2020
Edvin Hansson

Contents

Notation

Abbreviation	Meaning
CFD	Computational Fluid Dynamics
MVEM	Mean Value Engine Modeling
NARX	Non-linear Autoregressive Model with Exogenous inputs
DAE	Differential Algebraic Equations
CV	Control Volume
GUI	Graphical User Interface
VIGV	Variable Inlet Guide Vanes
VOGV	Variable Outlet Guide Vanes

Symbol	Meaning	Unit
$\dot{m}_a$	Air mass flow	kg/s
$\dot{m}_f$	Fuel mass flow	kg/s
$\dot{m}_g$	Combustion product mass flow	kg/s
$\dot{m}_{exh}$	Exhaust gas mass flow	kg/s
ω	Rotational speed	rad/s
Tq_c	Compressor consumed torque	Nm
Tq_t	Turbine generated torque	Nm
Tq_{load}	Load torque	Nm
Tq_{st}	Starter engine delivered torque	Nm
$\dot{m}_{in,i}$	Mass flow into control volume i	kg/s
$\dot{m}_{out,i}$	Mass flow out of control volume i	kg/s
P	Pressure	Pa
T	Temperature	K
Π_c	Pressure ratio across compressor	-
W_c	Compressor mass flow	kg/s
Π_t	Pressure ratio across turbine	-
D_c	Compressor stage diameter	m
η_c	Compressor efficiency	-
$N_{c,max}$	Maximum rotational speed	rpm
$\dot{m}_{c,corr,max}$	Maximum corrected compressor mass flow	kg/s
β	Auxiliary parameter in maps	-
$\Delta T_{i,j}$	Temperature difference between point i and j	K
c_p	Specific heat during constant pressure	J/kg
ω_{ign}	Speed at which ignition takes place	rad/s
ω_{curr}	current rotational speed	rad/s
M_i	Mass inside volume i	kg
c_v	Specific heat at constant volume	J/kg
R	Specific gas constant	J/kg K
V_i	Volume i	m^3
C_{tu}	Flow restriction tuning parameter	m^3/s
P_{us}	Upstream pressure	Pa
P_{ds}	Downstream pressure	Pa
ΔP	Pressure difference	Pa
J_{ax}	Rotational inertia of gas turbine	$kg \cdot m^2$
M_{ax}	Axis mass	kg
r_{ax}	Axis radius	m

1

Introduction

Gas turbines are come in a wide array of sizes and are used in just about as many different applications. What they all have in common is that they all consume some kind of fuel, and deliver power as output. Many aspects of the general design holds for most gas turbines: they consist of an air intake, a compressor sequence, a combustion chamber, and a turbine. All of this is attached to some form of rotating axis, generating a power output. There exists a few different axis configurations: one-, two- and three-axis turbines are available on the market. Some more specific features are variable inlet guide vanes that control the way the incoming air meets the compressor, and bleed valves that allows some of the compressed air to by-pass the combustion chamber and instead mix with the hot gases colliding with the first turbine blades.

When creating a simple, generalized model of how the parts are connected inside the turbine, the most important connections are the mass flows and the torque balance. The mass flows in a sense determine how much power is generated, which determines the rotation, which determines the flow. Figure 1.1 provides a basic overview of how the components interact inside the turbine. Note especially the mass flow path from left to right in the figure. The compressor block contains the air intake and produces an air mass flow that is provided to the combustion chamber block along with the fuel mass flow from the fuel injection control. These flows determine the combustion and a hot gas mixture flow moves downstream to the turbine. After passing the turbine, the flow continues into the exhaust system. Another aspect to observe is the torque dynamics which are parallel to the mass flow. The rotational speed ω is an important aspect in determining the flow and power inside the compressor and turbine blocks. In return, the power consumed and generated by these blocks, along with that generated by the starter motor and applied by the load torque, determine the rotational speed development.
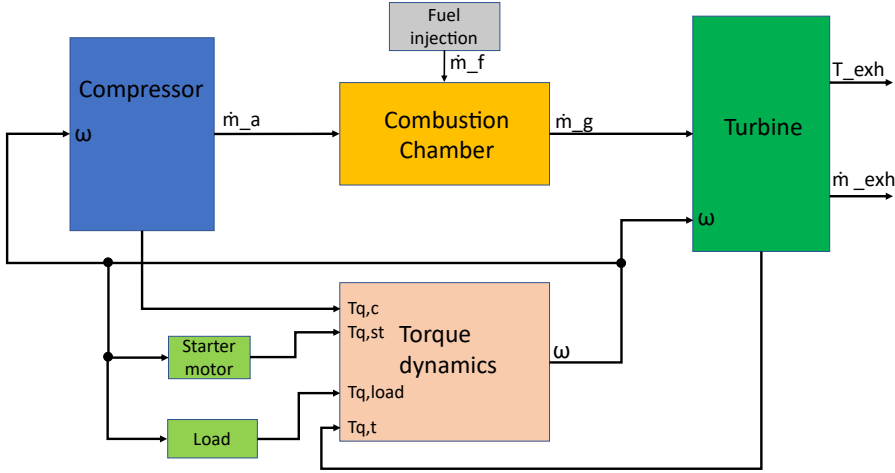
Figure 1.1: *Overview of the most important parts of the gas turbine and how they are connected. The compressor block contains a model of all its nine stages and outputs an air mass flow, $\dot{m}_a$ and power Tq_c to the combustion chamber and torque dynamics respectively. The combustion chamber block is fed fuel mass flow $\dot{m}_f$ and the air mass flow and the combustion model results in changes in temperature, pressure and exhaust gas mass flow $\dot{m}_g$. The turbine model uses exhaust mass flow to generate power, Tq_t. The turbine is also connected to the exhaust system and generates exhaust temperature T_{exh} and exhaust mass flow $\dot{m}_{exh}$. The torque dynamics is provided the generated powers from the starter motor, the load torque, the compressor and turbine and generates the rotational speed ω.*

The principles behind a gas turbine are quite simple. Its operation is best described using to the Brayton cycle. For more details on the operating principles, see Larsson [17]. In short, it can be described in three steps. First, the compressor compresses the air so that it reaches higher density, meaning that more air mass flows into the combustion chamber. Secondly, fuel is injected into the combustion chamber, where it is ignited and burns under constant pressure. Lastly, the energy released through the combustion is recouped in the turbine as the hot gas is expanded through the turbine. There is a fourth step linking the ambient conditions at the exhaust to the similar conditions at the intake.

The more you compress the incoming air, the more air molecules are available inside the combustion chamber, meaning that you can inject more fuel and still preserve a healthy fuel-to-air ratio. To allow for complete stoichiometric combustion of the injected fuel molecules, there must be enough oxygen available inside the combustion chamber for the hydrocarbons in fuel to react with during combustion. Should there be an insufficient amount of air, and subsequently oxygen, the exhaust gas mixture would contain carbon monoxide, rather than carbon dioxide. In terms of greenhouse gas emissions and environmental impact, this is highly undesirable. On the other hand, injecting too much air will decrease

the flame temperature, which according to Larsson [17] should be kept high, to maintain high turbine efficiency. In gas turbines, Larsson [17] states, the amount of air available during combustion is significantly larger than the stoichiometric value, leading to a very high combustion efficiency in general. This means that it is a sound assumption to consider the combustion stoichiometric, and that the exhaust gas only contains carbon dioxide, water vapor and any excess air. A gas turbine can be powered by many different fuels, depending on design choices. The most common fuels are natural gas and kerosene.
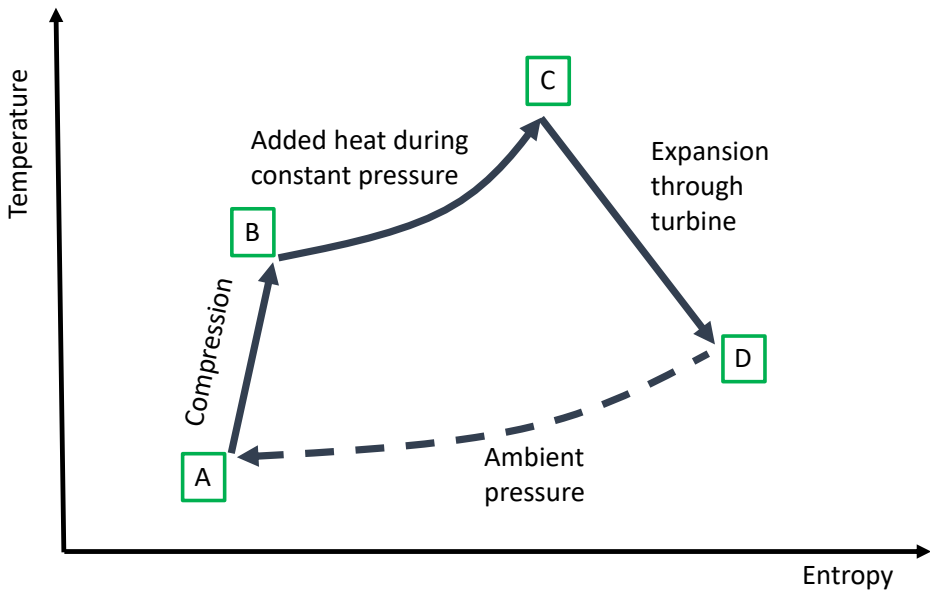

Figure 1.2: The Brayton cycle, as realized in a gas turbine.

The cycle is followed from A to D, as seen from the turbines intake to the exit. Along arrow A-B, the compression takes places inside the compressor, increasing the temperature of the incoming air. Arrow B-C describes what happens when the air flow reaches the combustion chamber. Burning injected fuel in practice means that heat is added to the gas mixture. The combustion process inside gas turbines are considered a constant pressure process, like a bunsen burner, for instance. When the hot gas mixture meets the turbine blades, it expands and work is performed on the turbine blades. This process is indicated by arrow C-D. Finally, the gas mixture is out in the ambiance again, with a slightly higher temperature than at the intake. Arrow D-A takes the process back to the intake with fresh, new air entering the gas turbine.

To operate a gas turbine is both time consuming and economically draining. There are large masses and inertia to overcome, as well as material stresses to avoid by adhering to temperature limits. This means that live testing during product development is an expensive activity. It is therefore highly desirable to have reliable and sufficiently detailed models for simulation purposes. One

important factor to consider when creating simulation models, is to make them as general as possible to ensure that they can be of use in as many situations as possible. On the other hand is this aspect counteracted by the fact that all gas turbines in operation in the field are unique individuals with their own quirks.

These two opposing aspects of model design means that a modular approach is a good compromise. This means that the gas turbine model can be separated into smaller sub-models, which all will contain parameters that can be adjusted to fit different gas turbine configurations and operating conditions. A general gas turbine model for simulation which allows for user defined variables and parameters has the potential to save both time and money during product development and research. While one trend in gas turbine simulation currently is pointing towards utilizing finite element methods and CFD (computational fluid dynamics) to intricately study and optimize design details, see for instance [26], there are other ways to model gas turbines.

The method of Mean Value Engine Modeling (MVEM) is a way of modeling presently used in the automotive industry. It is more or less the diametrical opposite of CFD, with MVEM focusing on mean values of temperatures, pressures and flows etc. while CFD is very detailed and intricate. The allure of CFD and its ability to predict exact temperature development in very precisely defined areas and volumes is ever-increasing, as the price of computational power is steadily dropping, meaning that the backside of demanding and time consuming mathematical operations is less of an issue. However, when simulating entire energy plants or larger gas turbine systems, MVEM has its merits, primarily due to simplicity and modularity. The MVEM framework is also well suited to be implemented in Matlab Simulink, which allows for easily accessible and user-friendly simulation of the gas turbine.

Within the MVEM model of the gas turbine, the compressor model will be crucial in determining the overall model performance. Another inspiration can be drawn from the vehicular (and maritime) industry here, as the Ellipse modeling procedure could be a useful way of modeling the gas turbine compressor stages.

1.1   Objective

The objective of this thesis is to create a model of a gas turbine in Matlab Simulink. The gas turbine compressor is comprised of nine stages, all individually modeled using Ellipse compressor model. The general design of the gas turbine follows the MVEM framework and intends to show that both MVEM and the Ellipse model can be exported from the vehicular industry and into gas turbines.

The aim is to study transient behavior in gas turbines, meaning that the gas turbine model is dynamic and not only designed for the simpler, steady state operation at the gas turbine design point, but should be able to handle surge and choke as well. This leads to further challenges during the modeling phase, especially as the functionality of the compressor and turbine is not defined in their respective component maps for these regions. However, using the Ellipse

model to represent the compressor stages should allow for some extrapolation into surge and choke operating regions.

When the model is in place, the goal is to simulate firstly steady state and secondly transient operation. During the simulated scenarios, values of temperatures, mass flows, pressures, torques and speed are logged and monitored, to allow comparison and evaluations of the model's performance.

1.2   Thesis outline

The thesis will start off by in Chapter 2 presenting some of the previous work in the field of compressor and gas turbine modeling and the major inspirations for the thesis. It contains a run-through of the most important papers and books that have impacted and influenced the thesis.

Next, a thorough description of the gas turbine model is given in Chapter 3. There is both an overview of the model and how everything looks at the top level, as well as in-depth description of each sub-system. The modeling chapter also contains explanations and motivations behind the made design choices.

Following on from the model description, Chapter 4 outlines the actual results of the thesis work. The chapter contains a table of the model errors from the Ellipse compressor model for all the nine stages, along with an evaluation. Furthermore, the results include an evaluation of the accuracy of the rules of thumb from [7]. Finally, the resulting output from the start-up scenarios are provided and analyzed from a few perspectives.

To round off the thesis, Chapter 5 is dedicated to drawing conclusions about the thesis work; what went well, what could have been better and what would be interesting future work, building on from this thesis?

1.3   Delimitations

This thesis or the model does not include any work on:

- Control of inlet- and outlet guide vanes

- Impact of temperature on gas constants

- Different fuels (even though this is easily adjusted)

- Gas turbine trips (failure and shut-down)

- Multi-stage turbine

- Multi-axis designs

- More or less than 9 compressor stages

The control of inlet and outlet guide vanes predominantly has to do with removing and recuperating swirl energy in the mass flow before and after the compressor. As this thesis implements a simple one-dimensional flow model, there is no

swirl energy taken into account. Modeling the impact of temperature on gas constants is also something that is normally done in more intricate models of more narrow scenarios. NASA polynomials are a common way of doing this, as indicated by Larsson in [17]. Any implementation of this, should also be coupled with a more detailed description of the gas mixtures inside the turbine, as well. If there was more computational power available and a more detailed model was desired, this could be a way of creating a more life-like model of the gas turbine. There probably are other things that would have a greater impact on the model accuracy, though.

Different starting points and conditions could also be of interest later on. Optimally, the model should handle starting from standstill, as it tests the model across the widest span of operating points.

Other gas turbine configurations, in terms of amount of axes or stages, is in principal just as interesting as the configuration in this thesis. Adding more axes and more stages would add complexity to the model, so keeping the model as minimal as possible, yet still relevant, was the goal.

2

Previous work

Since the thesis stands on the two primary legs of the Ellipse compressor model and dynamic gas turbine modeling as a whole, some previous work in the two fields are presented and commented on.

2.1 Ellipse Model and Compressor Maps

There have been multiple publications of different kinds during the development of the Ellipse model. Initially, it stems from the work performed by Oskar Leufvén during his PhD studies at the institution of Vehicular Systems at Linköping University. The first paper on the subject is [18] which describes the Ellipse compressor model concept. The authors cover the underlying idea of modeling a compressor across not only the normal operating region, but also including surge, choke and restriction operation. These three phenomena are described and it is motivated why it is desirable to model them. In automotive applications, transient operation is more of a rule than an exception, and it is not uncommon that vehicles are driven in such a way that the circumstances forces the compressor into sub-optimal operating regions. These scenarios are not as prevalent in literature regarding gas turbine operation - their compressor design is different. Gas turbines have axial compressors, while automotive and marine applications have centrifugal compressors.

There are other differences in design as well, for instance the fact that gas turbine compressors commonly consist of well over a dozen compressor stages, while automotive compressors normally are one- or two-staged. The principle is however still the same, and the compressor maps presented in [18] and [19] are similar to those seen in [14], while [2] points out that performance maps use corrected quantities in the gas turbine case. The use of corrected quantities is discussed in [18] as well. One notable difference in compressor maps for auto-

motive applications and those in gas turbines, is that the gas turbine maps also frequently normalize their axes with respect to the rated corrected quantity value due to their unwillingness to disclose absolute values.

Further work on the Ellipse model is found in the work of Llamas and Eriksson [20, 21]. Here, the compressor model is extended to utilize different parametrization methods and also include adiabatic efficiency extrapolation. The latter is of significance where the heat transfer effects are considerable - generally at low compressor speeds and mass flows, where the heat transfers more easily from the combustion process back to the latter stages of the compressor.

Initial work on axial flow compressors stems from two papers presented by Greitzer [8, 9], in which substantial research is done regarding the stall/surge behavior in axial compressors. These two papers are well-cited and have had a substantial impact on how surge is modeled in many other papers in the field.

Interesting work regarding scaling and extrapolating compressor models is found in the works by Eriksson et al. [7], where the authors device a few rules of thumb for compressor scaling. Some of these rules of thumb have been investigated in this thesis, to see whether their accuracy can be reproduced for axial compressors.

A related subject is the modeling of the turbine operation. Some of the foundation work on this subject (and for compressor modeling, as well) is found performed by Moraal and Kolmanovsky in [22], where thermodynamic expressions and assumptions are used to form accurate models for compressor and turbine performance.

The main reference on MVEM is the book written by Nielsen and Eriksson [5], which is mainly aimed at the vehicular modeling, but nonetheless provides information useful to this thesis, as well. Among other things, it contains some basic explanations regarding performance maps for compressors and turbines.

An alternative compressor map generation method, very similar to the Ellipse model, is presented by Yang et al. in [30]. This article was used as validation of the Ellipse model's suitability to also model gas turbine compressor maps, given that it is aimed at gas turbines - a field in which the Ellipse model had not yet been tried before this thesis. Yang et al. utilize a parametrization method very similar to the one used by Eriksson et al., with the aim of making mathematical functions, rather than look-up tables, the basis of the compressor model.

When modeling gas turbines, and especially compressors, the works of Kurzke [15] is essential. One of the most significant papers is the one by Kurzke and Riegler [14], where a way of scaling compressor maps is proposed. Much of the works of Kurzke and his co-authors are distilled in the gas turbine simulation program GasTurb13, which is very much at the forefront of gas turbine modeling. Other pointers on how to scale compressor maps are found in the paper by Rademaker [25].

The idea of taking an entire pack of compressor stages, and divide it into its constituent stages is seemingly not very common. In most models available in literature, multi-stage compressors are represented as look-up tables based on one compressor map for the entire compressor pack. Kurzke provides some thoughts about this issue in the manual for GasTurb13, but otherwise, the inner workings of multi-stage compressors are best covered by Koh and Ng [12]. The paper suggests a way of dissecting a multi-stage compressor at its operation point and provide some very important pointers as to how pressure is distributed among the stages inside the compressor.

2.2   Gas Turbine Modeling

There have been many articles and conference papers devoted to different aspects of modeling gas turbines. The challenge is to find research that is directly related to what is being investigated in this thesis. A well-cited and seemingly relevant article on the subject is the one by Kim et al. [11], where the authors both explain the fundamental parts of gas turbine modeling and propose models that could be of interest. Since the models are to be used to study transient behavior and control strategies, the models need to be dynamic. This means that many models based on steady-state operation data is of less interest and the basis for selection narrows. One relevant article is Asgari et al. [2] who have created a model of a heavy duty gas turbine in Simulink. The authors implement both a physics-based model and a black-box model using a non-linear autoregressive model with exogeous inputs (NARX), to good effect. Since the model in this thesis aims to be physics based, some pointers to useful equations is found here.

Notable work on gas turbine modeling is also found in the works of Larsson [16, 17]. His efforts were aimed towards creating a gas turbine model which could be used for supervision and informed decisions on maintenance and also contains relevant equations and motivations regarding the physical and thermodynamic properties of the gas turbine. Unlike Asgari et al., Larsson opted to create the gas turbine model in Modelica, motivating the choice with the fact that the gas turbine descriptions will lead to Differential Algebraic Equations (DAE's) and algebraic loops. The presence of algebraic loops is highly problematic when using numeric solvers, such as those commonly found in Matlab Simulink, according to Larsson [17]. This problem is not present when using Modelica, as one is able to define the causality between the sub-models and equations - breaking the algebraic loops and providing unique solutions. Larsson [17] also contains some important assumptions and guiding equations for the sub-models of the gas turbine.

Another possibly interesting paper on the subject of gas turbine modeling, even aimed at dynamic simulations, is the master's thesis by Turie [4]. Gas turbine modeling from a sub-model and modular perspective is also investigated by Yebra et al. in [31], who like Larsson opted for Modelica as their software of choice. A Simulink model of a gas turbine is found in the works of Patel et al. in

[24]. The paper is almost 25 years old and mostly aimed at aerospace applications of gas turbines, but the basic concepts are the same. Finally, the most relevant articles are the ones by Camporeale et al. [3] and Tsoutsanis et al. [28], where a Simulink model of a gas turbine aimed at dynamic simulation is the main focus in both papers. Especially [28] has been used as a foundation, as it uses a more familiar notation and the implementation of the gas turbine model was closer the case studied in this thesis. The model used in both articles uses differential equations describing the tracked states, as well as the conventional use of 2D-lookup tables for compressor modeling. This structure, paired with the data and real-life and insight from Kim et al. [11] was the main basis for the gas turbine modeling in this thesis. Some of the work by Rowen [1] is also closely related to the dynamic Simulink model of the gas turbine used in this thesis. Furthermore, Rowen provides conceptual controller designs which were used in this thesis. It also includes some field data used to validate the model in this thesis.

3

Model

This chapter describes the modeling procedure and the inspirations and reasoning behind the model structure. The complete gas turbine model consists of a number of sub-models for the different parts. At top level, the major subsystems are:

- The compressor

- The combustion chamber and fuel injection

- The turbine

- The torque dynamics

These subsystems then in turn consist of further subsystems containing the underlying control systems, governing equations or component maps which determine their functionality. All subsystems are connected with various signals as inputs and outputs, describing how the different parts of the gas turbine interact and depend on each other. Each subsystem will have its own in-depth description in its respective section below. Figure 3.1 provides a schematic overview of how the sub-models are connected inside the simulation model, as well as where different quantities and measurement signals are located.

3.1 Compressor model

The compressor model consists of nine different stages, separated by control volumes (CV's). The foundation for all stages is a common compressor map collected from Gasturb 13 that has been scaled in different ways. Inspiration for the scaling of the different stages is gathered from a paper on stage un-stacking [12]
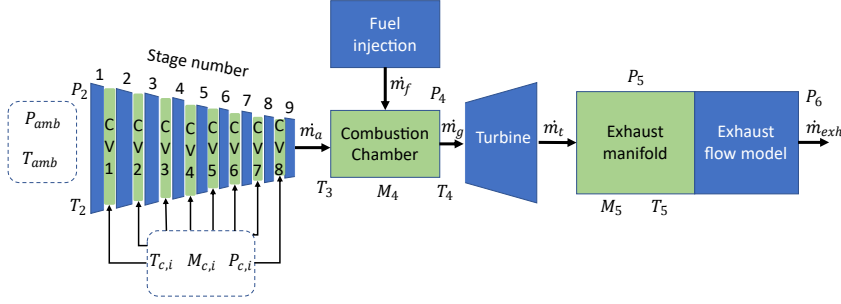
Figure 3.1: *An overview of the model structure and where different states and measurement signals are located in the model. Green blocks are control volumes and blue are flow generating models. The compressor model consists of nine stages separated by eight control volumes, where stage number one is at the air intake and stage nine is the last stage, at the compressor exit. The combustion chamber is a control volume, with the added input of the fuel flow. The pressures inside the combustion chamber and the exhaust manifold determine the pressure ratio across the turbine. At the exit, the exhaust flow model operates against P_6 which is modeled as a constant pressure, three bar above ambient.*

which indicates how one can scale the pressure ratio for each individual stage in a multi-stage compressor.

Compressor maps utilize corrected quantities to allow for a much simpler representation of the compressor performance across different conditions. Practically, in this thesis, corrected rotational speed is calculated using Equation 3.1 and corrected mass flow is found using Equation 3.2.

$$N_{corr} = \frac{N}{\sqrt{T_{us}/T_{c,ref}}} \tag{3.1}$$

$$\dot{m}_{c,corr} = \dot{m}_c \frac{\sqrt{T_{us}/T_{c,ref}}}{P_{us}/P_{c,ref}} \tag{3.2}$$

This means that the corrected quantity scales with the working conditions of the compressor stage and allows for representation of different compressor stage inlet conditions within a single map. In the multi-stage compressor model in this thesis, each compressor stage has its own reference temperature, $T_{c,ref}$ and reference pressure, $P_{c,ref}$. These are calculated using Equation 3.3 using the optimal operating point of each stage.

The generally most important features of the compressor is how it behaves in terms of pressure ratio, mass flow, temperature and power. Using the Ellipse model, a model is returned that on macroscopic level in terms of input and output can be described as $[W_c, \eta_c] = f(\Pi_c, N)$. There are a number of sub-equations used, see the works of Llamas and Eriksson [21] for further details.

Apart from that, the basic compressor equations governing the output temperature and power from a compressor or a compressor stage, are as follows:

$$T_{ds} = T_{us} \cdot \left[\frac{1}{\eta_c} \left(\frac{P_{us}}{P_{ds}} \right)^{\frac{\gamma_a - 1}{\gamma_a}} - 1 \right] \tag{3.3}$$

$$P_c = \dot{m}_c \cdot \Delta T \cdot c_{p,a} \tag{3.4}$$

Where $\Delta T = T_{ds} - T_{us}$, the temperature difference between upstream and downstream of the compressor stage. Furthermore, η_c is the compressor stage efficiency, P_{us} and P_{ds} are the pressures upstream and downstream of the compressor stage and γ_a is the ratio of specific heats for air, $\gamma_a = c_{p,a}/c_{v,a}$.

3.1.1 The Ellipse compressor modeling procedure

When constructing the compressor stage by stage, there were a few things to consider. The four most significant are total pressure ratio, maximum mass flow capacity, number of stages and total power output.

The total pressure ratio and the number of stages are actually two of the few things easily available from gas turbine companies and their websites. This made the first step quite easy, along with the total power output, which is frequently used in sales-pitches and the first thing you learn about a gas turbine. The power output can vary, depending on how you implement the gas turbine on site and what auxiliary components are used. The most common options of implementations are whether the turbine is used directly for a mechanical driving purpose or for power generation.

Some gas turbine manufacturing companies also provide information regarding the exhaust mass flow and temperature, which provide convenient benchmarks for evaluating the entire gas turbine model.

What is not common to find, is the compressor- or turbine maps. This is of course very reasonable, since this is proprietary information and well-kept company secrets in most cases. What makes it even more difficult to retrieve such data, is that even in academic applications, commercial gas turbines are used and maps are rarely presented. The best one usually can hope for, is outdated information from compressors and turbines that present no current fiscal value for the company behind it.

The task in this compressor modeling project, was to take a multi-stage compressor and divide it into its individual stages. This is rarely done, as in any commercial or academic implementation, what usually matters is how the entire pack of compressor stages perform together as a unit. In this thesis however, it was decided that it would be interesting to try and break a multi-stage compressor down into a series of compressor maps of individual stages and intermediate control volumes, as depicted in Figure 3.2. In order to obtain a realistic compressor map of a single stage, the gas turbine performance software program named GasTurb 13 was used.
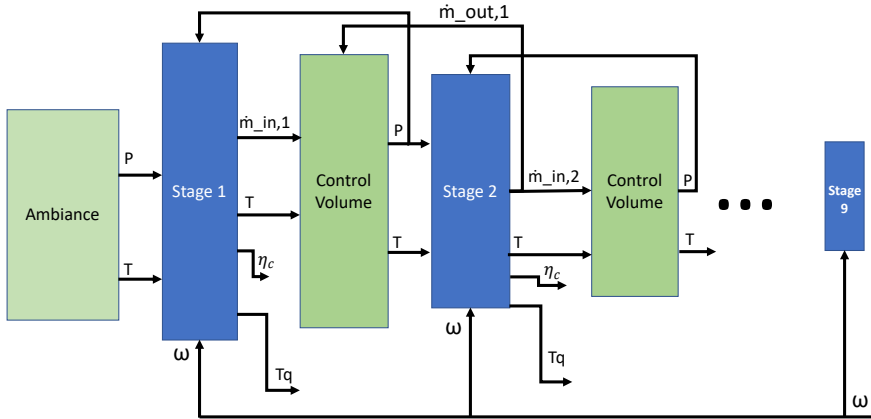
Figure 3.2: *Simplified model of the structure of the multi-stage compressor. The blue blocks are the Ellipse model of each stage, which produce mass flow ṁ, temperature T, efficiency η_c and torque Tq depending on the pressures and temperatures in the upstream and downstream control volumes, along with the rotational speed ω. The control volumes develop pressures and temperatures depending on incoming and outgoing mass flow and temperatures from the upstream and downstream compressor stages.*

The program allows the user to build, simulate, alter and dissect many different gas turbine configurations, using the extensive work by Kurzke and Riegler [14] as a foundation. Along with the program, some basic maps are included. One of these is a *fan map*, a compressor map of a single compressor stage in a jet engine. The principles are the same in jet engines and gas turbines for other applications, so the map is generally representative of one stage in a multi-stage compressor.

Preprocessing and scaling

The map was transferred to MATLAB for pre-processing and validation of the map's resemblance to other known compressor maps. Firstly, the efficiency data was filtered to only contain points in the range of [0,1], which led to the removal of the two lowest speed lines. What remained was a compressor map with documented speed lines of 50, 60, 70, 80, 90, 95, 100 and 110 % of rated speed. The value of rated speed was not disclosed in the map. Instead, based on the model in Tsoutsanis et al. [28], it was set to 10000 rpm.

The original map can be seen in Figure 3.3. The map also points out the surge and choke lines and regions. Here, the bad efficiency data has been filtered out, but no scaling has been performed. After this, the flow axis was scaled to match the design exhaust mass flow listed in the Siemens SGT-750 [27]. All compressor stages were scaled identically in this dimension.

When the original map was deemed a valid representative of a single compressor stage, and the flow scaling was done, the pressure ratio scaling followed.
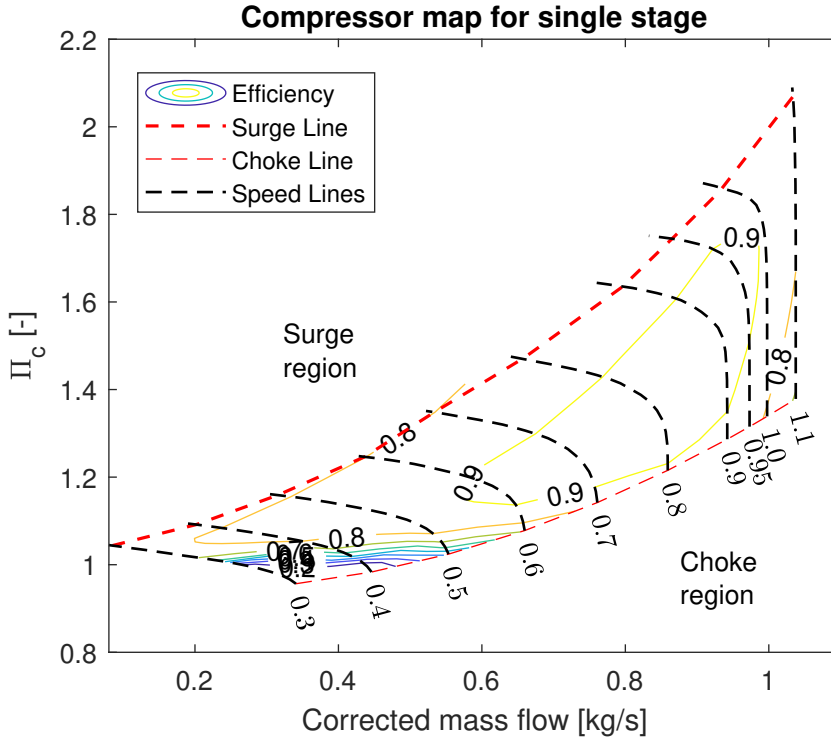
Figure 3.3: *The original compressor map after preprocessing is a good example of a general compressor map. The speed lines are 50, 60, 70, 80, 90, 95, 100 and 110 % of rated speed and each is drawn in a different color, with the lowest speed at the bottom and left and speed rising towards the upper right corner. The highest efficiency is found at 0.8 to 0.9 times rated speed. Note the surge line limiting the speed lines in the upwards, leftwards direction. Similarly, the choke line ends the speed lines towards the bottom right, and beyond it is the choke region.*

To maximize the likelihood of having a good match between the different stages' pressure ratio, inspiration was taken from previous research in the field. According to some hints, rules of thumb and field data in [12] and [7], a pressure ratio profile was constructed. In practice, this is a curve of the pressure ratio available at each stage in the compressor. There are several ways to look at available pressure ratio and how it is connected to the resulting total pressure ratio: firstly, one can study the optimal pressure ratio at rated speed. This means that you multiply the pressure ratio at which the stage delivers the highest efficiency at rated speed. This way of studying the pressure ratio distribution provides insight as to where the turbine's optimum working point will be, and if there are any abrupt pressure changes between adjacent stages. Secondly, there is the option of studying the maximum pressure ratio at the highest speed line in the map. This instead provides information as to what the capacity of the compressor is. Depending on what the turbine is used for, the two viewpoints may be of varying relevance.

Since the goal for this thesis is to study transients, there is more focus on the operating range of the compressor, rather than the optimal operating point during steady state. This lead to the implementation of the model in [12] which modeled the maximum stage pressure ratio. In principle, the model can be approximated as a linear decrease of maximum available pressure from the stage closest to the inlet, to the last stage stemming from the width of the stages. The front stages are larger and wider and have a higher maximum pressure ratio, and both stage width and maximum pressure ratio decrease almost linearly from front to end. A linear approximation of the pressure ratio model in [12] is made, and then applied to the nine-stage compressor model used in this thesis. The pressure model and the linear fit is shown in Figure 3.4a, and the pressure ratio curve used in this thesis is shown in Figure 3.4b.

This generally follows the field data presented in [12], with a higher pressure ratio at the inlet (stage number one), and increasingly lower towards the compressor outlet, at stage nine. The difference that can be seen between the model in [12] and the one in this thesis, is that the former has more, smaller stages, while the latter has fewer but larger.

LiU CP GUI modeling process

When the preprocessing and scaling procedure was finished and the resulting maps were deemed to be the nine different scaled compressor maps were fed to the program LiU CP GUI to create Ellipse models of the compressor stages.

The general procedure of the Ellipse modeling of the compressor maps can be seen in Figure 3.5a and Figure 3.5b, where the two steps in the modeling are depicted. In Figure 3.5a the flow model is shown. Here, the "Ellipse"-part of the name becomes clear to see, as the elliptic shape of the speed lines are used as a base for the mathematical representation of the compressor map. Figure 3.5b shows the typical parabolic shape of the efficiency as a function of mass flow for each speed line. The tool contains the possibility of fitting and adjusting the elliptic shape and curvature to the input map, which proved crucial to the model fit.
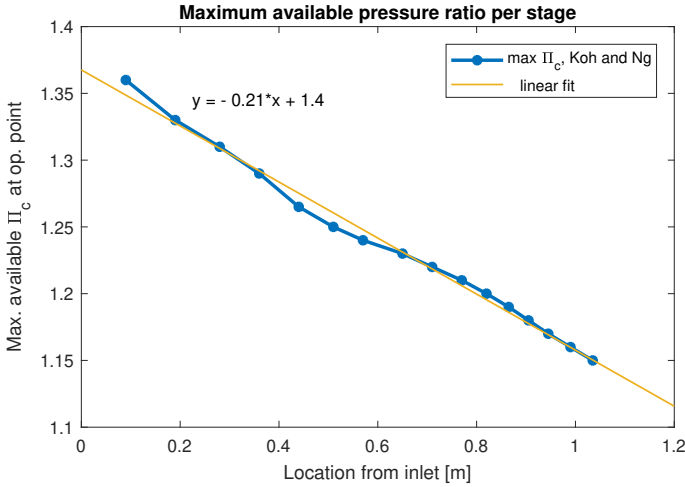
(a) *The pressure ratio model from Koh and Ng [12]. There is a clear linear trend showing that the maximum pressure ratio available at a stage decreases the further it is located from the inlet, and the shorter the stage width is.*
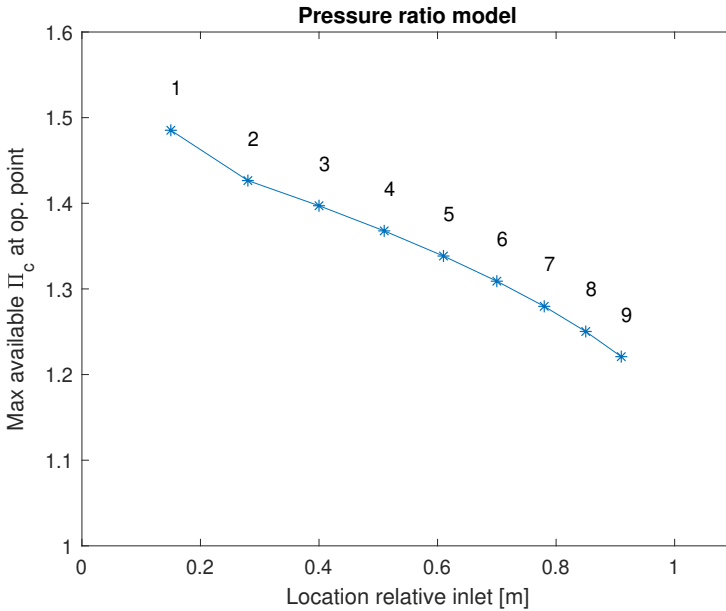

(b) *The pressure ratio model used in this thesis. There are fewer stages in the model than in [12], but the linear trend of maximum pressure ratio and stage width produces a similar pressure ratio curve.*

Figure 3.4: *Pressure ratio distribution model from [12] along with its linearized fit, which was used as basis for the pressure ratio distribution in this thesis.*
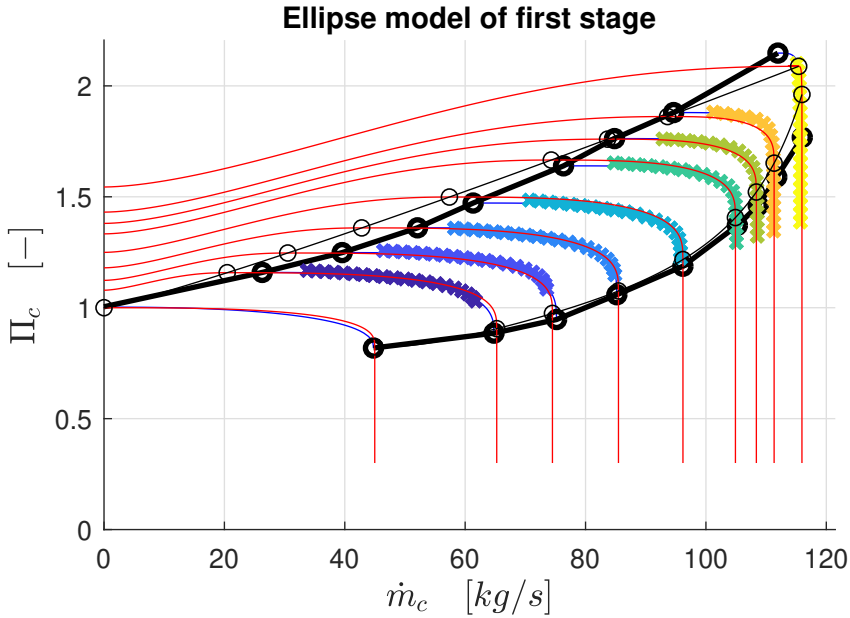
(a) *The Ellipse flow model. Thick colored lines are the input speed line data. The red lines are the fitted curves of the Ellipse model. Black circles can be moved around by the user to create desired curvature on model lines. It can be seen that the red lines of the Ellipse model pass through the speed lines provided in the map, which is desirable.*
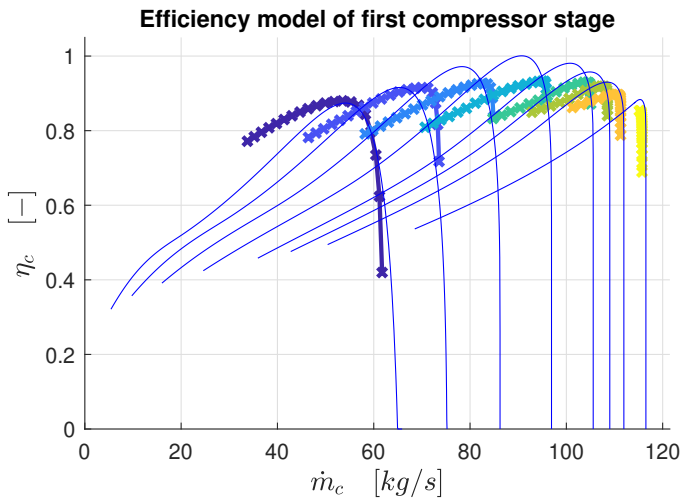
(b) *The efficiency model. Thick lines are input data, blue lines are the fitted efficiency model. The efficiency model fit is not great for all stages, as exemplified by the fact that one of the lines exceeds efficiency of 1.*

Figure 3.5: *The two parts of the Ellipse modeling procedure.*

The program returns models and errors in two stages: first, the Ellipse flow model provides a model of flow and pressure ratio, then secondly, a total model is generated, containing efficiency as well as flow and pressure ratio. LiU CP GUI returns parameters for each sub-model, as well as the sub-model's mean absolute relative error and maximum absolute relative error. Both are given in percent. The output parameters then can be saved and used inside Simulink block representations of the compressor stage.

3.1.2   Rules of thumb

To aid in the design of the compressor stages in terms of diameter, some inspiration was drawn from the rules of thumb presented in [7]. The three rules of thumbs were as follows:

$$\Pi_c = 6.2 \frac{2}{\pi} \arctan(20 D_c) \tag{3.5}$$

$$N_{c,max} \approx \frac{515}{D_c \pi} 60 \tag{3.6}$$

$$\dot{m}_{c,corr,max} = \left(D_c \frac{6}{0.74} \right)^2 \tag{3.7}$$

Obviously, it should be noted that these rules of thumb were created based on a database of centrifugal compressors from the automotive and marine industry. While they are still compressors, there is a difference in design and working principle.

The first rule is in a sense the most interesting one, since the individual stages can have both their own pressure ratio and their own impeller diameter. On the other hand, it is stated in [7] that there is little physical basis for the first rule of thumb, so there might not be any greater connection between that rule of thumb, and the results in this thesis, as the compressors used are fundamentally different in the two cases.

For rules two and three, there are complications as to how to implement them. In a multi-stage compressor, the idea is that at steady state, all stages should deliver the same amount of air mass flow, and as they are all mounted on the same axis, the rotating speed is the same for all stages. One solution to this dilemma could be to find some average diameter to represent the compressor pack. What is encouraging about the other two rules of thumb, is that these are more founded in physical relations between quantities. It is reasonable to believe that the mass flow is proportional to the square of the impeller diameter, as it should be proportional to the cross-section area. Similarly, the relation between impeller diameter and maximum rotational speed has its basis in that the impeller tip speed being found to be fairly constant across different compressor sizes in [7].

3.2   Turbine model

The turbine model is in essence a look-up table. It is based on a map from Gas-Turb and processed and scaled to fit the best operating point of the compressor. The original turbine map was from a significantly smaller turbine, in terms of both pressure ratio and mass flow. The scaling procedure was performed so that the maximum efficiency spot of the turbine map was located at the same pressure ratio and mass flow as that of the compressor. This was done by scaling both mass flow and pressure ratio axes individually. The scaling procedure was performed in accordance to the well-established rules in Kong et al. [13].

The scaling of the mass flow is a simple linear scaling with the ratio between the desired design point mass flow and the old design point mass flow:

$$\dot{m}_t = \frac{\dot{m}_{des}}{\dot{m}_{des.old}} \dot{m}_{old} \tag{3.8}$$

The scaling of the pressure ratio is a little more intricate:

$$\Pi_t = \frac{\Pi_{t,des} - 1}{\Pi_{t,des.old} - 1} \left(\Pi_{old} - 1 \right) + 1 \tag{3.9}$$

In both equations, subscript des indicates the new map's desired design point value, des, old indicates the original map's design point value and subscript old denotes the old map quantity. In essence you take the old map, subtract one from the pressure ratio, scale it with the ratio between the new and old design point pressure ratios, and then add one again. Kong also provides a simple linear scaling of the turbine efficiency, but there is no such scaling performed in this thesis. The resulting turbine map is shown in Figure 3.6.

The Simulink model of the turbine contains sub-models for:

- Efficiency

- Generated mass flow

- Output power

- Output temperature

The inputs to the turbine model are:

- Pressure upstream (combustion chamber)

- Pressure downstream (exhaust manifold)

- Rotating speed

These quantities are used as input to a number of look-up tables which are used to follow the standard used in GasTurb for representing the turbine maps. The most notable feature of their representation of the maps, is the so-called β-parameter, an auxiliary parameter which takes a value between 0 and 1. Figure 3.7 gives an overview as to how the turbine model is connected.
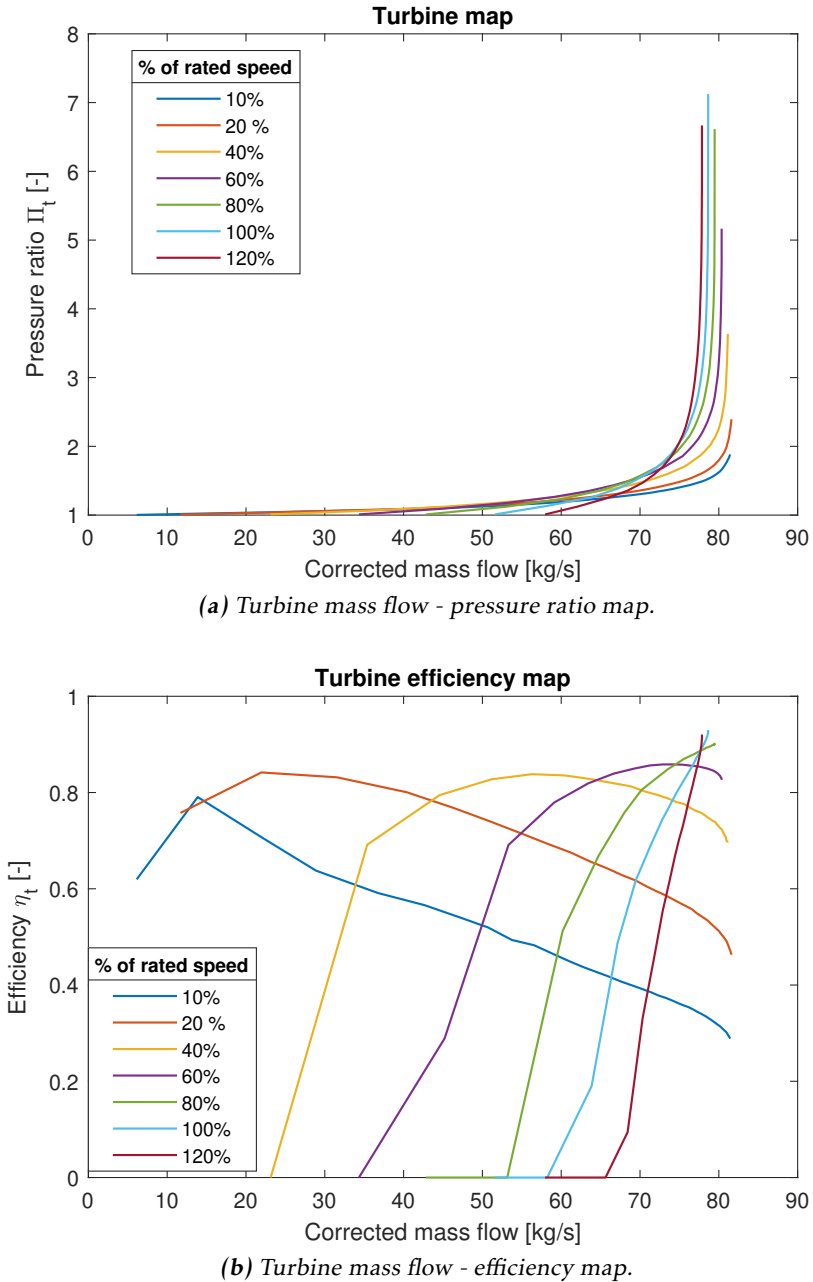
(a) Turbine mass flow - pressure ratio map.

(b) Turbine mass flow - efficiency map.

Figure 3.6: *Turbine maps, depicting relations between mass flow, pressure ratio and efficiency for different speed lines.*
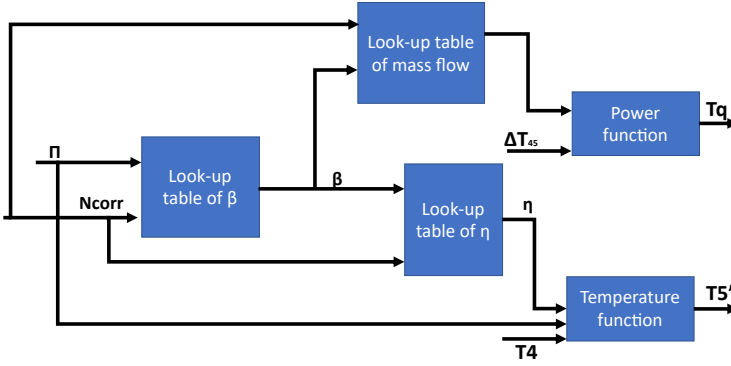
Figure 3.7: *An overview of the turbine Simulink model.*

The turbine maps are defined so that for every given combination of rotational speed and β, there is a single output value of mass flow. The value of β is derived from the current rotational speed, for which there is a specified maximum and minimum pressure ratio. The β value is a representation of where on the interval between these two points, the current pressure ratio across the turbine, lies. If the pressure ratio is at it maximum for the current speed, $\beta = 1$, while $\beta = 0$ is the case for minimum pressure. This means that the speed provides maximum and minimum pressure through one look-up table, and then maximum and minimum pressure ratio, along with current pressure ratio provides β. Another look-up table then returns the corrected mass flow when inputting β and corrected rotational speed.

The efficiency model is also retrieved from GasTurb in the form of a look-up table. This is provided corrected rotational speed and β as input, and provides efficiency as output.

Mass flow and efficiency then provides the output power and temperature by the basic turbine equations:

$$T_5 = T_4 \cdot \left[\frac{1}{\eta_t} \left(\frac{P_5}{P_4} \right)^{\frac{\gamma_g - 1}{\gamma_g}} - 1 \right] \tag{3.10}$$

$$P_t = \dot{m}_t \cdot c_{p,g} \cdot \Delta T_{45} \tag{3.11}$$

where $\Delta T_{45} = T_4 - T_5$, the temperatures inside the combustion chamber and at turbine exit, respectively. Furthermore, P_4 and P_5 are the pressures inside combustion chamber and exhaust manifold. Finally, η_t is the turbine efficiency and $c_{p,g}$ is the specific heat of the gas mixture passing through the turbine.

In principle, it can be seen in Equation 3.11 that the most power is retrieved from the turbine when the mass flow is high and the temperature drop is large. To achieve a large decrease in temperature after the turbine, it can be seen in Equation 3.10 that the efficiency should be high.

3.3   Combustion model and fuel injection

The combustion model is retrieved from Tsoutsanis et al. [28] and is essentially a pure energy accumulation equation based on the input variables:

- Incoming Air mass flow, $\dot{m}_a$

- Incoming Fuel mass flow, $\dot{m}_f$

- Outgoing mass flow, $\dot{m}_g$

- Inlet temperature

- Exit temperature

The equation is similar to the ones used in the control volumes, an unsteady flow equation with the added energy in the form of the injected fuel mass.

$$\dot{T}_4 = \frac{[h_b - c_v(f/a)\cdot T_4]\cdot \dot{m}_a + [Q_{LHV}\cdot \eta_b - c_v(f/a)\cdot T_4]\cdot \dot{m}_f - [\dot{m}_g\cdot R_g(f/a)\cdot T_4]}{M_4 c_v(f/a)}$$

(3.12)

Here, $h_b = c_p \cdot T_3$, the burner enthalpy, Q_{LHV} is the lower heating value of the fuel injected and η_b is the burner efficiency, which is assumed to be constant at 98 %. Furthermore, M_4 is the mass currently residing inside the combustion chamber which is calculated as $\dot{M}_4 = \dot{m}_a + \dot{m}_f - \dot{m}_g$. Gas constants R, c_v and c_p are functions of the fuel to air ratio, f/a.

When assessing Equation 3.12, there are three clear terms in the numerator and one expression in the denominator. Firstly, $[h_b - c_v(f/a)\cdot T_3]\cdot \dot{m}_a$ denotes the temperature change related to the incoming air mass flow. Secondly, $[Q_{LHV}\cdot \eta_b - c_v(f/a)\cdot T_4]\cdot \dot{m}_f$ is the temperature change induced by the injection of fuel. Note that this is zero if the fuel mass flow is zero. It can also be noted that a high burner efficiency and high lower heating value of the fuel, results in larger temperature increase for a given amount of fuel. The last term in the numerator is related to the mass flow leaving the combustion chamber, $\dot{m}_g \cdot R_g(f/a)\cdot T_4$. Note that this term has a minus sign, which means that a high mass flow leaving the combustion chamber, makes the temperature drop. The former two terms impact the temperature positively when the flows are large. Lastly, the expression in the denominator, $M_4 c_v(f/a)$, acts as some form of inertia. With a large mass inside the volume, the changes in the numerator have less impact on the temperature.

The fuel injection controller design is inspired by the work of Rowen [1] and is controlled by a double PI-controller. The first controller uses the speed error rated speed – current speed as input and providing a mass fuel flow in kg/s as output. The other controller is based on controlling the turbine exit temperature - one of the more critical quantities in the gas turbine. The reference temperature curve is taken from Kim et al. [11] and provides the goal temperature for a certain speed. As indicated originally by Rowen in [1], and also by Kim et al. in [10], the selection of which of the two control signal to use, is performed by a simple minimum selector. This maintains a continuous control signal and allows a safer

and more modest control strategy. It also makes economical and ecological sense, as it is preferable to use as little fuel as possible.

The fuel is assumed to be mostly methane, as is the case in natural gas. The work performed by Park et al. in [23] indicates that it is reasonable to assume that approximately 90-95% of the content of the natural gas is methane in that case. Furthermore, it is stated in [23] that the typical fuel-to-air ratio is approximately 1/50 for natural gas in gas turbines. Park et al. also state that the lower heating value of the natural gas in that case is $42.71 MJ/Nm^3$. The unit used is energy per normal cubic meter, a quantity commonly used when referring to gases, as their properties change with temperature and pressure. A normal cubic meter is the amount of gas that fits inside a volume of one cubic meter at atmospheric conditions. The density of natural gas at standardized conditions is normally in the region of $0.7 - 0.9 kg/Nm^3$. Using the higher of these two values leads to the lower heating value of the fuel in the model being assumed to be 47.5 kJ/kg.

Discarding the approximately 5% of the fuel that consist of other substances than methane, the combustion process is simply burning methane at constant pressure, with access to an excess of air. The combustion process for methane with a excess of air available is shown in Equation 3.13. Here, air is considered to be composed of 79 vol.% nitrogen and 21 vol.% oxygen, leading to 3.76 mass fractions of nitrogen per mass fraction of oxygen. All other components of the air are neglected.

$$CH_4 + 2\left(O_2 + 3.76N_2\right) \leftrightarrow 2H_2O + CO_2 + 7.52N_2 \tag{3.13}$$
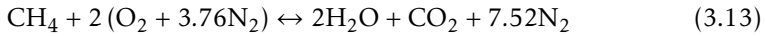
This leads to the assumption that the exhaust gases downstream of the combustion chamber consists of two parts water vapor, one part carbon dioxide and 7.52 parts nitrogen in terms of molar composition. Combining the assumption about the fuel-to-air ratio, the air composition and the combustion formula provides the specific gas constant of the exhaust gases, which is needed when calculating the pressure inside control volumes. The general equation for the gas constants can be written as

$$
\begin{aligned}
R_g = 3\left[\frac{1}{\frac{1}{f/a}+1}\right] \cdot \left[2 \cdot R_{H_2O} \cdot M_{H_2O} + R_{CO_2} \cdot M_{CO_2} + 7.52 \cdot R_{N_2} \cdot M_{N_2}\right] \cdot \\
\left[\frac{2}{M_{H_2O}} + \frac{1}{M_{CO_2}} + \frac{7.52}{M_{N_2}}\right] \cdot \frac{1}{2+1+7.52} + \left[\left(\frac{1}{f/a}-2\right) \cdot \frac{R_{air}}{\frac{1}{f/a}+1}\right]
\end{aligned}
\tag{3.14}
$$

In principle, the reaction is considered to be that of one part fuel and 1/(f/a) parts air. From one part fuel, there is 3/(1/(f/a) + 1) parts exhaust gas, and (1/(f/a) - 2)/(1/(f/a) + 1) parts air in the combustion product. In the normal case, as per Park et al. [23], $f/a = 1/50$, which means that there is one part fuel and 50 parts air. The combustion product then becomes 3/51 exhaust gas and 48/51 air. The long expression in the middle of Equation 3.14 stems from the conversion between moles and mass, as the model as a whole uses mass as basis, but the combustion equation is performed in moles. So, R_{H_2O}, R_{CO_2} and R_{N_2} is in [J/mol K] and then M_{H_2O}, M_{CO_2} and M_{N_2} is the molar mass, unit [moles/kg].

The equation is identical for $c_{p,g}$ and $c_{v,g}$, it is just a matter of replacing R_{H_2O}, R_{CO_2} and R_{N_2} with their respective $c_p and c_p$ values.

Finally, there is a delay inserted in the fuel system model to account for the inertia inside both the fuel distribution system and the gas exchange. This delay is modeled as a first order transfer function with a time constant of 0.5, as indicated by Rowen [1].

3.4   Load Torque modeling

To take the gas turbine between operating points and to keep it at desired speeds, the load torque is applied. This is done by a simple P-regulator that applies the difference between the generated torque from the turbine, and the consumed torque from the compressor. Inspired by Rowen [1], there is an added torque which is deducted from the load torque to create a positive net torque, leading to a controlled acceleration. Figure 3.8 contains a schematic view of the load torque controller.
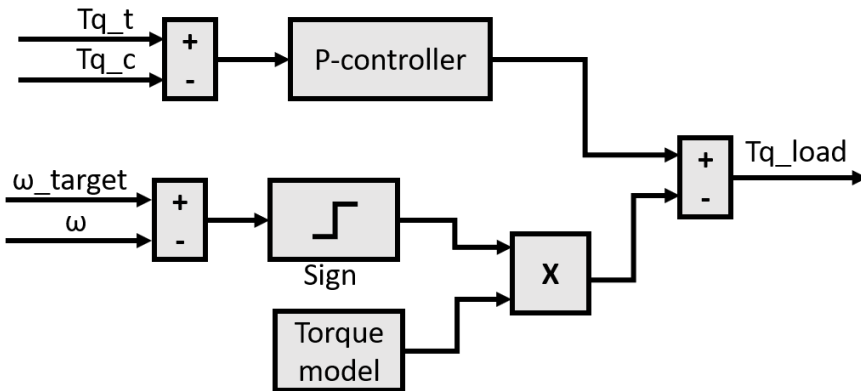
Figure 3.8: An overview of the load torque model.

The load torque model has its upside in its ability to maintain a stable net power acting on the axis, as neither peaks or drops in either compressor or turbine power affects the rotational speed notably. The downside of this, is that the dynamic relation between flow, pressure ratio and rotational speed is cut off. In the end, the model sacrifices its resemblance with reality in order to increase its controlability. In Chapter 4.5, the load torque model is reconstructed to be more lifelike.

3.5   Mean Value Engine models

The mean value engine modeling framework is a way of modeling which origi-
nally was aimed at vehicles. The basis for the MVEM used in this thesis is built
on the work by Eriksson et al. in [6] and [5]. The modeling structure is intention-
ally not as detailed or cumbersome calculation-wise as Finite Element Methods,
and the focus is on having a model framework that provides calculations and
values as averages across engine cycles in combustion engines. Common imple-
mentations are diagnosis or control systems and depending on usage area, the
time-frame for the updates is in the range of 0.1-50 Hz, according to [5].

The MVEM framework is well suited to control system applications, as it is
not overly concerned by small, local and short-lived phenomena, but rather the
mean values across (relatively) larger time frames. This also means that MVEM
is a valuable asset in some diagnosis applications. Given that the principles in-
side vehicles in terms of gas flows, combustion, temperatures, pressures and even
torque dynamics are very similar to those inside gas turbines, the MVEM frame-
work should be fit for purpose here as well.

The MVEM framework builds on two main building blocks in terms of gas
flow: the control volume and the flow restriction. Both are described in their
own sub-sections below, sections 3.5.1 and 3.5.2 respectively. Finally, the MVEM
applies a common torque dynamic model based on input torques and an rota-
tional inertia of the gas turbine, described in subsection 3.5.3.

3.5.1   Control volumes

The control volumes are models of manifolds and spaces with fix volume. The
manifolds are viewed as thermodynamic control volumes, storing mass and en-
ergy. In practice, this is easily converted to provide values of pressures and tem-
peratures inside the volumes, which are more relevant to the model. The dynamic
behavior inside the volumes is based on a set of differential equations:

$$\dot{M}_i = \dot{m}_{in} - \dot{m}_{out} \tag{3.15}$$

$$\dot{T}_i = \frac{1}{M_i c_v} \left([\dot{m}_{in} \cdot \left(c_p T_{in} - c_v T_{out} \right)] - [\dot{m}_{out} \cdot R \cdot T_{out}] \right) \tag{3.16}$$

$$P = \frac{M_i \cdot R \cdot T_i}{V_i} \tag{3.17}$$

Equation 3.15 is simply the mass state equation. The change in mass inside
the volume is given by the difference between incoming and outgoing mass flow.
Equation 3.16 describes the temperature change inside the volume. The inputs
are: incoming mass flow $\dot{m}_{in}$, with temperature T_{in}, outgoing mass flow $\dot{m}_{out}$,
current temperature inside the volume, T_{out} and M_i, the mass currently residing
inside the volume. For control volumes inside the compressor model, the gas
constants c_p, c_v and R are considered to be constant, but from the combustion

chamber and downstream towards the exit, these are instead functions of fuel to air ratio.

Equation 3.17 describes pressure development and is an extension of the mass state equation, using the assumptions that the medium inside the volume is an ideal gas. Using the specific gas constant R, temperature inside the volume T_i and the fix volume V_i, the pressure can be calculated.

The equations are implemented so that the Simulink block containing (3.16) provides the integrated value of $\dot{T}$ and the integrated value of M to the block containing (3.17).

3.5.2 Flow restriction

The flow restrictions are based on the assumption that the flow inside the gas turbine is turbulent and incompressible. Incompressible flow is an adequate assumption in cases where the Mach number of the flow is not higher than approximately 0.2-0.3, according to [5]. Given the size and scale of a gas turbine, there are indications that the Mach number is higher than that throughout most passages in the turbine. The information in [29] points towards the only place of approximately sufficiently low Mach number, is in the exhaust manifold. Even here, there are indications that it could be higher, so ideally, the flow should be modeled as compressible. This would however require more field data from actual gas turbine, while the incompressible flow model only has one tuning parameter to consider, giving a simpler model:

$$\dot{m} = C_{tu} \cdot \sqrt{\frac{P_{us}}{R \cdot T_{us}}} \sqrt{\Delta P} \tag{3.18}$$

Where P_{us} and P_{ds} are the pressures upstream and downstream of the restriction, respectively. Further, $\Delta P = P_{us} - P_{ds}$, R is the specific gas constant and T_{us} is the temperature upstream. The tuning parameter, C_{tu} is used to provide reasonable flow based on the pressure relation between upstream and downstream of the restriction.

It can be seen that the incompressible, turbulent flow model runs into problems when the pressure upstream is no longer higher than that downstream. That situation gives Δp less than zero, meaning that the square root returns a complex number, causing the simulation to crash. This situation should not occur in reality, as the pressure ratio should be comfortably on the correct side at the location of the flow restriction model; the pressure in the manifold immediately after the turbine should be comfortably higher than what is almost atmospheric pressure at the exit, downstream of the restriction. According to an assumption made by Asgari et al. in [2], the pressure in the exhaust system is 3 bar above ambient during turbine operation at rated speed.

3.5.3　Torque dynamics

The torque dynamics are represented by a simple differential equation:

$$\dot{\omega} = \frac{\mathrm{Tq}_t + \mathrm{Tq}_{st} - \mathrm{Tq}_c - \mathrm{Tq}_{load}}{J_{ax}} \tag{3.19}$$

It is a simple torque balance; the torque from the turbine, Tq_t and the starter Tq_{st} are defined to accelerate the axis when positive, while the torque from the compressor, Tq_c and the load torque, Tq_{load} are defined to be braking the axis when positive. The rotational inertia of the axis, J_{ax}, is modeled as that of a simple cylinder:

$$J_{ax} = \frac{M_{ax} r_{ax}^2}{2} \tag{3.20}$$

Where M_{ax} is the mass of the axis, assumed to be 10 000 kg, r_{ax} is the radius of the axis, which is calculated as the mean radius of the compressor, which is 0.525 meters. This gives an inertia of almost 1400 kg m^2. The simplification of using a cylinder as a model means that the shape of the axis is assumed to be uniform, which is not the case in reality, where the axis is thicker at some places and thinner at others.

4

Results

This section presents how the model performed in simulations, with an initial description of the compressor model and compressor map in Chapter 4.1. It contains a description of how the map was created through simulations, and the resulting map is compared to the original, one-stage fan map that was the basis for the nine stages. The model map is also compared to one retrieved from GasTurb 13.

Chapter 4.2 contains a run-through of the model errors. First, the model errors from the Ellipse-modeling procedure are presented. The chapter also contains the resulting compressor diameter in the model, which is compared against the estimations based on the rule of thumb equations.

After that, the results of the simulated scenarios of steady state and transient behavior are presented in Chapter 4.3. The chapter contains discussions on how the model behaves and how the controller strategies are performing. Based on observations from these results, a new controller design is proposed, implemented and evaluated in Chapter 4.5.

4.1 Multi-stage Compressor

The multi-stage compressor was mapped out and tested in a simulated test-bench in Simulink. The compressor model was fed an array of different rotational speeds where it should function well. Essentially, it was the same speedlines as in the individual stages: 50, 60, 70, 80 , 90, 95, 100, 110 % of rated speed, which is 10 000 rpm. The pressure ratio increased from 1.5 up to 59.9 with a step size of 0.2. There was also a limiting check to see whether the pressure ratio was reasonable in relation to the rotational speed used. This was done by finding the maximum pressure ratio for each stage for the given speed. The product of these nine maximum pressures were used as an initial indicator of a surge-limit.
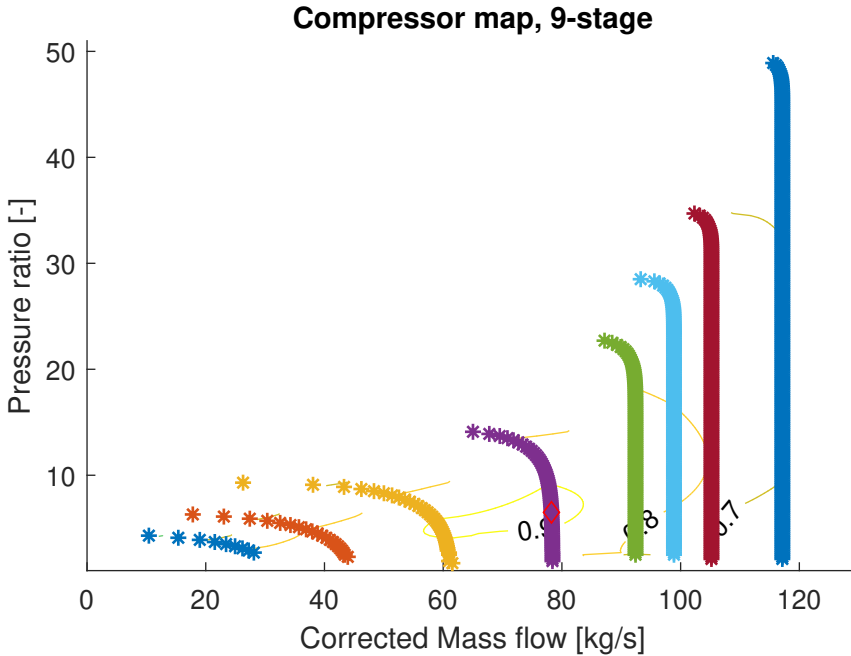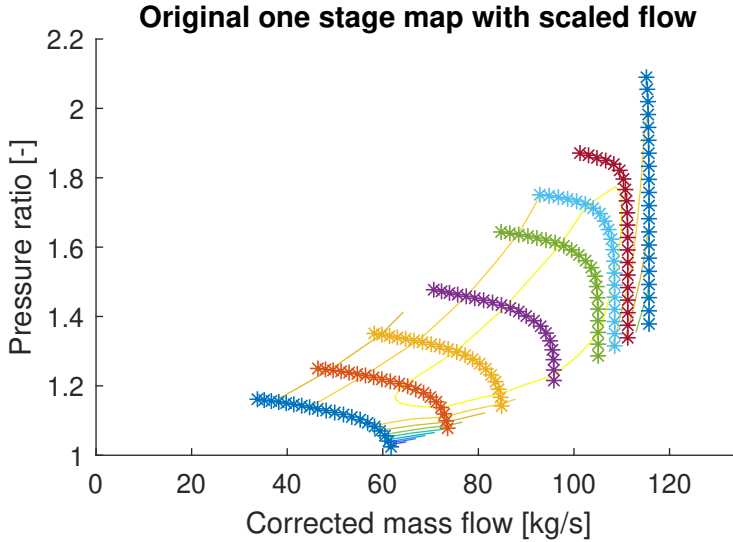
Figure 4.1: *Resulting nine stage compressor map. The speed line of 50% is the blue line in the bottom left corner, followed by 60 % being the red line, 70 % being the yellow, 80 % is the purple line, 90 % is green, 95 % is the light blue, 100 % is burgundy and 110 % is the vertical, darker blue. The simulated point with the highest efficiency is marked with a red diamond on the 80 % line.*

However, it was found that the multi-stage compressor could sometimes operate in regions significantly above the indicated surge line. To avoid unnecessary simulations, obviously inside choke or surge region for the given speed, a limit was imposed at four times the indicated surge pressure. Conversely, the minimum mapped pressures for the individual stages formed a theoretical choke line, but here it was also found that the multi-stage compressor could operate a fair bit below in many cases. To avoid simulating too low pressure ratios, however, there was a limit at 50% of the indicated choke pressure. The complete compressor map is shown in Figure 4.1. Each speed line is drawn in its own color.

The map indicates that the optimal efficiency region is at $[W_{c,corr}, \Pi, N_{c,corr}] \approx [80$ kg/s, 7, 8000 rpm]. It is clear that the optimal speed is somewhere between 7000 and 8000 rpm since that region results in the highest efficiencies. It is also clearly visible that 50% was a reasonable lower cut-off for the speed, as the behavior at lower speeds becomes very hard to map. At the other end of the spectrum, the speed line at 110 % of rated speed (dark blue, furthest to the right in Figure 4.1)

Original one stage map with scaled flow

Figure 4.2: *Original stage compressor map. The speed line of 50% is the three blue stars at the bottom left corner, followed by 60 % being the red line, 70 % being the yellow, 80 % is the purple line, 90 % is green, 95 % is the light blue, 100 % is burgundy and 110 % is the vertical, darker blue.*

is almost entirely vertical, indicating that the limit of the compressor is reached in terms of speed and mass flow, as it is almost invariant of pressure ratio.

To provide some context, Figure 4.2 depicts the map of the original stage, which was scaled nine different times to create the constituent stages. The similarity can be seen in where the optimum is located in terms of speed, although the single stage map has a wider region of high efficiency. Naturally, the pressure ratio is of smaller magnitude, but the mass flows are of the same order. A difference can be noted in the shape of the map, as the map gets slimmer and more narrow when the pressure ratio and number of stages increase.

Another relevant comparison to make, is to study the output from a more established and professional map-scaling and -generating program. Therefore a map was created in GasTurb 13 of a compressor of the same scale in terms of pressure ratio and mass flow. Figure 4.3 shows the map retrieved from GasTurb.

There are some immediate differences that can be noted: the efficiency is lower overall, and the high efficiency region is located much closer to the 1.0 times rated speed line. The highest efficiency in the GasTurb map is located between 0.85 and 1.0 times rated speed, with the optimal region seemingly between 0.9 and 0.95. It can also be seen that the compressor map from GasTurb is not at all as competent at coping with high pressure ratios. At 1.05 times rated speed, the red surge line pressure ratio is approximately nine, while the compressor in
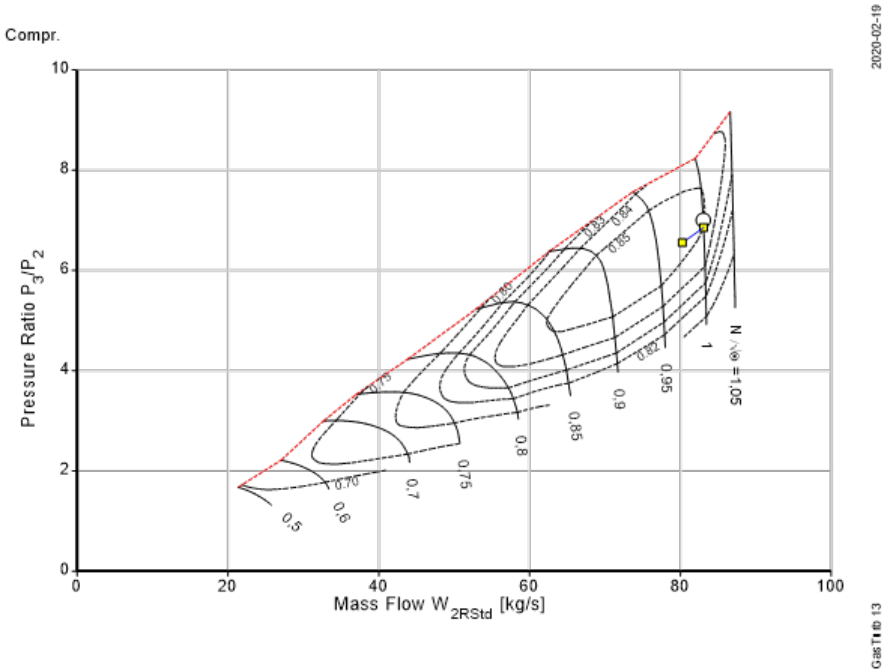
Figure 4.3: *Compressor map generated in GasTurb.*

the model in Figure 4.1 reaches pressure ratios of 30-50 between 100 and 110 % of rated speed (the two rightmost speed lines).

Otherwise, the speed lines are of a little different shape: the ones in the model in Figure 4.1 are quite vertical and do not bend leftwards towards the lower flow region as much as the ones in the GasTurb map do in Figure 4.3. Both maps have the same lower speed cut-off, with the lowest speed line being a short and quite horizontal speed line at 50 % of rated speed in both cases.

There seems to be a difference in the flow scaling, as the flow obtained at the highest efficiency point in the model map (the red diamond in Figure 4.1) is the same as the flow at 1.0 times rated speed in the GasTurb map. This probably stems from ambiguous interpretations of what the term "design point" means.

4.2   Model Accuracy

The most interesting aspect of the model is how accurate it is and if any systematic flaws can be detected. Since the model as an entity is a combination of several sub-models retrieved from a number of different sources, the main interest is to study errors in the sub-models. The main possibility to validate the entire model,

Ellipse Model				
-	Π_c		$\dot{m}_{c,corr}$	
Stage nr.	Mean abs. rel. error [%]	Max abs. rel. error [%]	Mean abs. rel. error [%]	Max abs. rel. error [%]
1	0.5994	3.3026	0.1998	0.9779
2	0.5282	1.8739	0.2770	1.5773
3	0.5077	1.8072	0.2912	1.3479
4	0.6499	3.7098	0.3167	1.2897
5	0.9362	2.8323	0.3111	1.5619
6	1.3477	3.7549	0.2607	1.3684
7	1.7857	4.5881	0.2556	1.4540
8	0.9512	5.5956	0.3802	2.4810
9	1.4643	5.5470	0.2594	1.1919

Table 4.1: *The model errors of the Ellipse compressor model. The errors are calculated using a Total Least Squares method and are measured as orthogonal 2D-distance between the fitted curve and the measurement points in the (mass flow, pressure ratio)-plane.*

is by looking at macroscopic outputs that are readily available, such as exhaust flows and power output. This is performed later in Chapter 4.4.

4.2.1   Ellipse model

The Ellipse modeling work resulted in model errors for the nine different maps that were input into LiU CP GUI. Table 4.1 contains the model errors of the Ellipse flow model and Table 4.2 lists the model errors of the entire model, which includes efficiency as well.

Generally, the mean absolute relative model errors are in the order of 1-4 %, which is good. There are no real outliers, but in terms of the complete model, stage number two has the worst mean fit and largest maximum error for both pressure ratio and efficiency. It does have the best fit in both mean and maximum terms for the mass flow, so it is not the worst in every sense. It can be noted that the errors are consistent and of similar magnitude across all stages, indicating that the size of the compressor stage is not a significant factor in the model fit.

4.2.2   Rules of thumb

When investigating how well the assumptions and model parameter values corresponded to the rules of thumb for automotive and marine compressors proposed

Complete model errors					
-	Π_c		$\dot{m}_{c,corr}$		η_c	
Stage nr.	Mean abs. rel. error [%]	Max abs. rel. error [%]	Mean abs. rel. error [%]	Max abs. rel. error [%]	Mean abs. rel. error [%]	Max abs. rel. error [%]
1	2.2763	11.9274	2.5472	10.3374	1.1515	3.7956
2	4.2501	20.3496	0.3338	1.6108	2.9502	10.5410
3	3.2702	17.8998	1.5861	4.3597	1.9647	5.8018
4	3.8711	17.6080	0.5270	2.0539	2.4839	6.1516
5	2.8631	14.9289	2.1374	6.4736	1.1054	3.6556
6	2.6258	13.7729	2.1443	7.8400	0.9543	3.2686
7	2.7780	14.1447	2.0718	7.5703	1.0404	3.4140
8	2.4748	11.7671	2.1918	9.2828	0.9540	3.3991
9	2.5457	12.0019	2.1895	8.7476	1.0079	3.8455

Table 4.2: *Model errors of the complete compressor model from LiU CP GUI. Here, the complete model is a Total Least Squares minimization across the three dimensions (mass flow, pressure ratio, efficiency) and errors are measured orthogonal distance in 3D between fitted curve and measurement points.*

in [7], there were three different rules to consider, which all could be rewritten to provide an estimate of the compressor impeller diameter.

$$D_{c,i} = \frac{\tan(\Pi_{c,i} \frac{\pi}{2 \cdot 6.2})}{20} \tag{4.1}$$

$$D_c \approx \frac{515}{N_{c,max} \pi} 60 \tag{4.2}$$

$$D_c = \sqrt{\dot{m}_{c,corr,max} \frac{0.74}{6}} \tag{4.3}$$

Since the diameter estimates are based on the data in the compressor maps, the stage diameter estimates based on mass flow $\dot{m}_{c,corr,max}$ and maximum rotational speed $N_{c,max}$ are the same for all stages. The diameter estimates based on maximum pressure ratio, $\Pi_{c,max}$ are unique for each stage, which is indicated by the use of the sub-index i in Equation 4.1.

Table 4.3 presents the rule of thumb estimates of the diameter for each stage and the model value of the stage diameters used in the simulations. Furthermore, Table 4.3 provides the absolute relative error between the simulation model value and that of the three rules of thumb for each stage. Absolute relative errors are calculated as in Equation 4.4.

$$\text{Abs. rel. err.} = \left| \frac{\text{Model value} - \text{Rule of thumb diameter estimate}}{\text{Rule of thumb diameter estimate}} \right| \tag{4.4}$$

Rule of thumb errors							
	D_c based on Equation 4.2 [m]	D_c based on Equation 4.3 [m]	$D_{c,i}$ based on Equation 4.1 [m]	Model diameter value [m]	Abs. rel. error [%]		
Stage number					$N_{c,max}$	$\dot{m}_{c,corr,max}$	$\Pi_{c,max}$
1	0.9836	1.3267	0.0295	1.5	50.79	23.00	> 100
2	-||-	-||-	0.0281	1.39	39.73	8.07	-||-
3	-||-	-||-	0.0274	1.28	28.66	6.85	-||-
4	-||-	-||-	0.0267	1.16	17.60	21.78	-||-
5	-||-	-||-	0.0260	1.05	6.53	36.70	-||-
6	-||-	-||-	0.0253	0.94	4.53	51.63	-||-
7	-||-	-||-	0.0247	0.83	15.60	66.55	-||-
8	-||-	-||-	0.0240	0.71	26.66	81.48	-||-
9	-||-	-||-	0.0234	0.6	37.73	96.40	-||-

Table 4.3: Model errors of the rule of thumb compared to the actual diameter values used in the simulation models.

It can be seen that the maximum speed estimate holds pretty well for the middle stages. The estimate of a 0.9836 m diameter would a little bit larger than stage six in the model, but not quite as large as the stage five diameter. Based on the rule of thumb in Equation 4.2, the maximum rotational speed in the model should be a bit lower to fit with the bigger stages, and higher to fit better with the smaller stages. If one uses the middle stage as an average representation of the entire compressor pack, the fit is very good.

The diameter estimate based on maximum mass flow is also quite accurate. It estimates the diameter at 1.3267 m, which is quite close to the values of the larger stages in the model; it would slot in between stage two and three in size. The general physical principle of the mass flow through an opening being proportional to its cross-section area - and consequently the square of the diameter - of course holds here as well. The difference between axial and centrifugal compressors should impact the tuning parameters in the rule of thumb Equation 3.7, though.

Finally, it can be seen in Table 4.3 the estimate from the maximum pressure ratio was very inaccurate. It is worth pointing out that this particular rule of thumb was a curve fit, and had no actual physical representation other than it being reasonable that larger compressors should be able to generate higher pressure ratios, given that increasing the diameter means an increase in volume compared to sur-

face. Less surface per volume would mean smaller impact from heat exchange
and friction, proportionally.

4.3   Simulations

The simulation of the start-up procedure contained many sub-tasks being ful-
filled and many parameters being tuned before it was stable enough to function.
Since the compressor, in particular, is sensitive to surge and choke, the need for
a smooth and well-controlled start-up was of utmost weight. The scenario was
this: start the gas turbine in a good operating point where both compressor and
turbine provide good efficiency according to their respective maps. From this
point, the first scenario was to accelerate the gas turbine only slightly, and then
hold the speed and reach steady state. The second scenario was a transient onto
the next speed line at 9000 rpm from the same starting point as the first simula-
tion.

The simulations were performed using the ODE23s solver in Matlab Simulink.
Stationary simulations and transients who reach steady state were performed
across a simulation time of 3600 seconds. The absolute tolerance was set to "auto",
which means that it is initialized to the relative error times 10^{-3}. Relative toler-
ance was set to 10^{-5}, which means that the absolute tolerance was initialized to
10^{-8}.

4.3.1   Initialization

When starting the Simulink model in an operating point, the initial values of
many signals are of utmost importance. To match flows, pressures and tempera-
tures as well as possible at startup, the compressor model was isolated and fed the
initial conditions for rotational speed and downstream pressure and the settled,
steady state signals were saved to Matlab and used as initial conditions for the
complete Simulink model simulations. This ensured that the compressor started
in a stable state with matching initial flows between the compressor stages and
their respective control volumes. The control volumes were initialized with tem-
peratures matching the reference temperature of the nearest downstream com-
pressor stage. These respective reference temperatures were calculated from
Equation 3.3, iteratively from stage one to nine, using the upstream stage output
temperature as input to the next stage, along with the optimal operating point in
$[\Pi_{c,i}, \eta_{c,i}]$.

Based on the initial pressures inside the compressor control volumes, the com-
bustion chamber initial pressure, mass and temperature was determined. From
there and further downstream, the turbine determined the initial conditions in-
side the exhaust manifold. Since the pressure inside the combustion chamber
now was deemed set, the pressure ratio across the turbine was determined by the
pressure inside the exhaust manifold. The initialization algorithm sets the pres-
sure inside the exhaust manifold to put the turbine in its optimal operating point
in terms of efficiency, given the set starting speed. A check is also implemented

to prevent the starting exhaust manifold pressure being below atmospheric pressure.

Finally, these initial values where used when starting the complete model. The model converged and stabilized after a few seconds, and all states that needed initial values were exported to Matlab and saved. These could then be loaded and used as initial values throughout the simulation process.

4.3.2   Steady operation

When testing and tuning the fuel injection, it becomes clear how complex the system is, and how everything is connected. When changing the fuel mass flow, the gas mixture in the exhaust gases is altered from the combustion chamber and downstream towards the exit. This in turn impacts the temperature and pressure development in control volumes, which affects the both compressor and turbine. This means that sound and stable control of fuel injection is critical for the stability of the simulation.

The test of the fuel control was performed by starting the gas turbine near its optimum operating point. All mass and temperature states inside all control volumes were initialized so that pressure ratios were reasonably distributed for the given starting point, as described in Chapter 4.3.1. Using the load torque control, the gas turbine speed was increased by 30 rad/s in a space of little over five seconds, and then kept at that speed. Figure 4.4 depicts the speed and power during transient and steady state after reaching the target speed.

It can be seen that the rise in speed is quite rapid and that in this operating range, the turbine generates approximately 25-30 MW more power than the compressor consumes.

The load torque speed control governs how much of the excess power is allowed to accelerate the turbine, and when the target speed is reached, the load torque follows the difference between compressor and turbine power. This means that the fuel control mostly serves as a way to hold temperatures, pressures and flows within desired ranges. Figure 4.5a depicts the fuel control signals and Figure 4.5b shows the fuel to air ratio during this scenario.

The fuel flow is very modest and is completely decided by the speed controller, which outputs a low fuel flow. The temperature control would prefer a higher fuel mass flow, as the temperature at turbine exit is quite low, but the minimum selector makes sure that the speed control signal is used. This makes for a quite low fuel to air ratio. Figure 4.6 depicts some important quantities inside the combustion chamber, to highlight how the fuel flow impacts the combustion process.

It can be seen that the low fuel to air ratio impacts the gas parameters, as R decreases. Notable is also the significant rise in mass, temperature and pressure inside the combustion chamber, perhaps motivating the decrease in fuel mass flow.

The pressure development inside the combustion chamber decides what downstream pressure and pressure ratio the compressor has to adhere to. All too sudden pressure rises are known to lead to surge. Figure 4.7 shows the compressor operating curve during the simulation. It can be seen that the initial operating
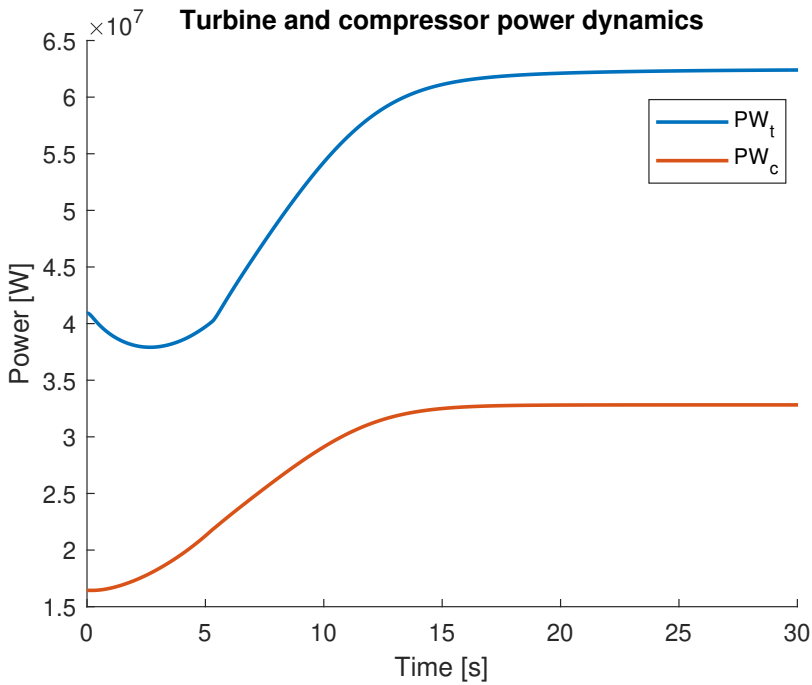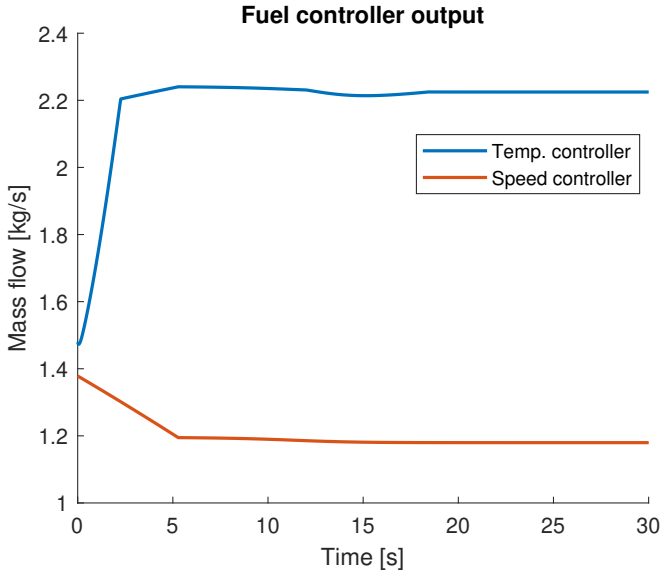
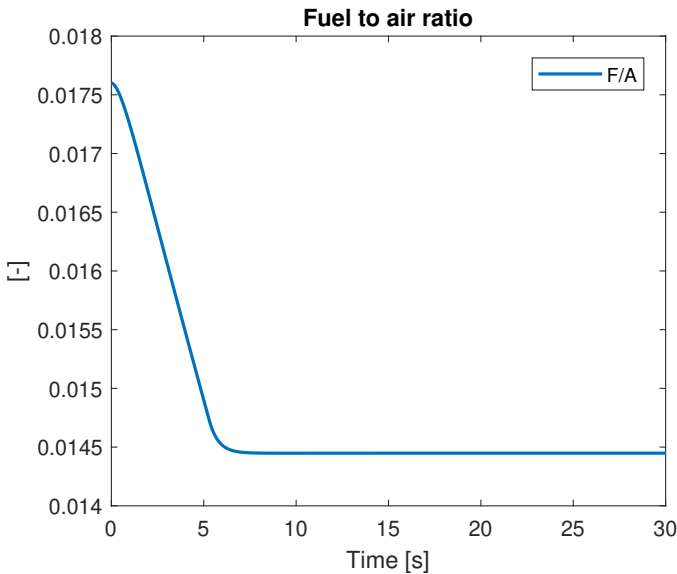(a) *Power development during 30 rad/s transient onto steady state.*
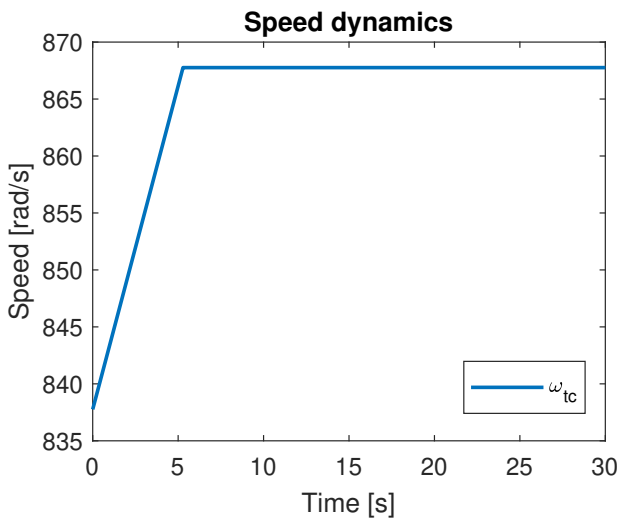
(b) *Speed development during 30 rad/s transient onto steady state.*

Figure 4.4: *Speed and power development during 30 rad/s transient and hold.*

Fuel controller output

*(a) Fuel controller signals during 30 rad/s transient onto steady state.*

Fuel to air ratio

(b) Fuel to air ratio during 30 rad/s transient onto steady state.

Figure 4.5: *Fuel mass flow controller signals and fuel to air ratio during 30 rad/s transient and hold. Note that the temperature controller outputs a significantly larger control signal than the speed controller. Since the resulting control signal is determined by a minimum selector, it is the speed controller that determines the fuel mass flow.*
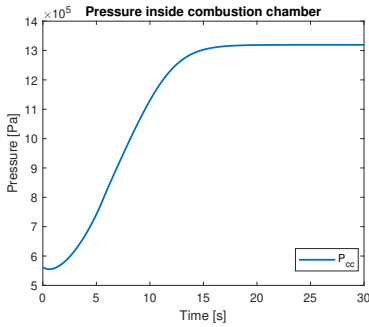
(a) *Combustion chamber pressure.*
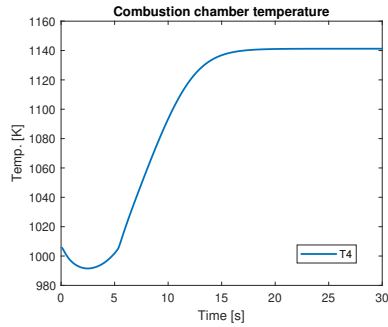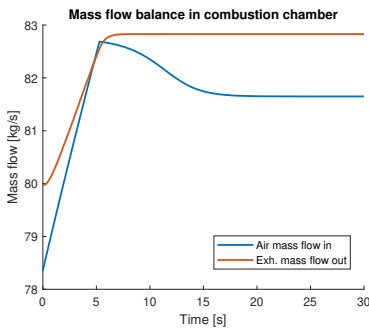
(b) *Combustion chamber temperature.*

(c) *Incoming air mass flow and outgoing exhaust flow.*
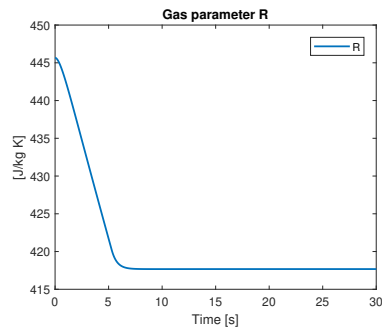
(d) *Specific gas constant R for gas mixture inside combustion chamber.*

Figure 4.6: *Development of various quantities inside the combustion chamber during 30 rad/s transient and hold. Most have similar shape as the speed transient.*

point is located inside the high efficiency region. The acceleration then takes the compressor upwards, towards the surge limit, but manages to stay below surge pressure ratio quite comfortably.
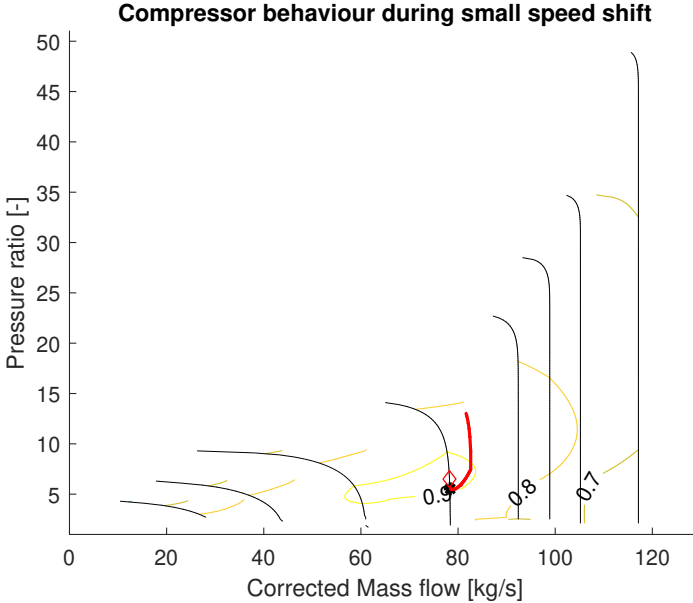
Figure 4.7: *Compressor behavior during 30 rad/s transient. Red curve is compressor operating points, red diamond indicates highest efficiency point. Black lines are the mapped speed lines. Black dot indicates starting point.*

This indicates that the pressure development inside the combustion chamber might be on the border of being too rapid in relation to how fast the speed increases, along with the air mass flow. Still, the gas turbine manages to hold an operating point into steady state operation.

4.3.3 Operating point shift

After confirming that the gas turbine could be controlled to maintain an operating point, the next step was to shift from one operating point to another. During transients, it is crucial to maintain stable behavior in terms of speed and temperatures to ensure minimal damage to the turbine.

The transient chosen was a larger speed increase of 1000 rpm, starting from the same operating point as in Section 4.3.2. The step was made by the load torque controller, which allowed some of the positive net torque in the relation $Tq_t - Tq_c$ drive the acceleration. Essentially, the fuel controller is used to try to

keep the conditions for the compressor, combustion chamber and turbine within functioning limits, while the load torque control is responsible for the rotational speed. This is not a very lifelike implementation, but it manages to create two separate controlling problems, rather than intertwining temperatures, flows and pressures with the speed dynamics. The one bond remaining is to try and match the speed increase to the pressure ratio across the compressor, as rotational speed is an important factor in compressor operation.

There were some adjustments made to the model to fit the larger transient simulation, rather than the task in Chapter 4.3.2. Namely, the controller parameters in the PI-controller for the fuel injection based on speed error needed tuning, as the speed error was larger in this simulation than in Chapter 4.3.2.

Figure 4.8 depicts the speed and power development during the transient. In Figure 4.8b it can be seen that the speed increase is very sudden, while Figure 4.8a shows that the net power generated fluctuates during the transient. Initially, the turbine power output is much larger than that consumed by the compressor. During the acceleration, the difference decreases before settling at a relation of approimately the same size as initially. Another point here, is that the detachment between the generated net power and the speed development is clearly visible, as the speed reaches its target and stays there thanks to speed control, while the fuel injection along with turbine and compressor power generation still changes.

Figure 4.9 shows the fuel control signals and fuel to air ratio during the simulation.

The fuel control signals clearly show that it is the speed control signal that is the decisive one, once again. The fuel mass flow requested due to temperature error at turbine exit would suggest that the fuel mass flow should be two or three times higher than what the speed error demands. There is a upper saturation at 3 kg/s, which the temperature control reaches, while the speed control orders a fuel mass flow of a steady decline from 1.4 down to approximately 0.8 kg/s. This leads to a fuel to air ratio that drops even below 1.5 %, well below its normal value of 2 %. This of course impacts the situation inside the combustion chamber. Figure 4.10 shows the most crucial quantities and signals inside the combustion chamber.

It can be seen in Figure 4.10a and Figure 4.10b that the drop and recovery-shape from the power development is also present here. It seems to stem from a sudden increase in outgoing mass flow, as can be seen in Figure 4.10c at approximately 80 seconds. Meanwhile, the drop in fuel to air ratio makes the gas constant R drop significantly. How the pressure drop and subsequent rise impacts the compressor is clearly visible in Figure 4.11.

Figure 4.11 shows how the compressor starts off in a high efficiency region. From there, both flow and pressure rises until the operating point reaches and follows the 9000 rpm speed line towards the surge limit, but stopping marginally before moving into surge. Ideally, the pressure ratio should not increase that much after reaching the desired speed, as it lowers efficiency and risks surge. The problem seems to be that the pressure in the combustion chamber keeps rising even after
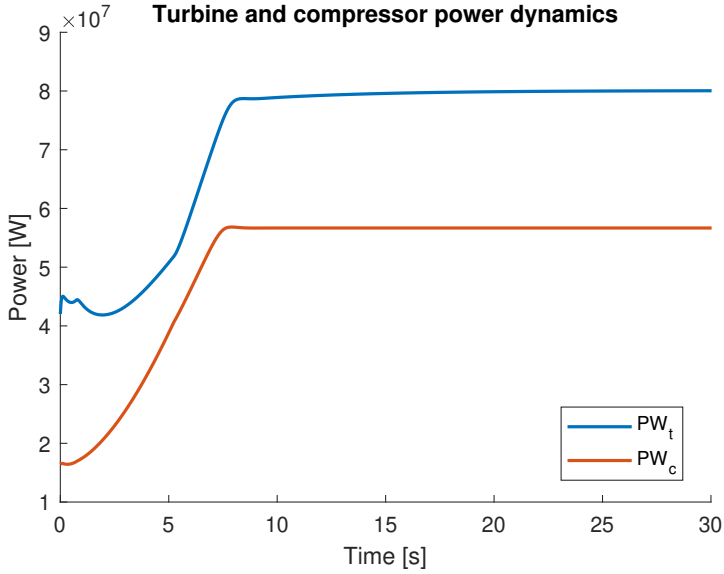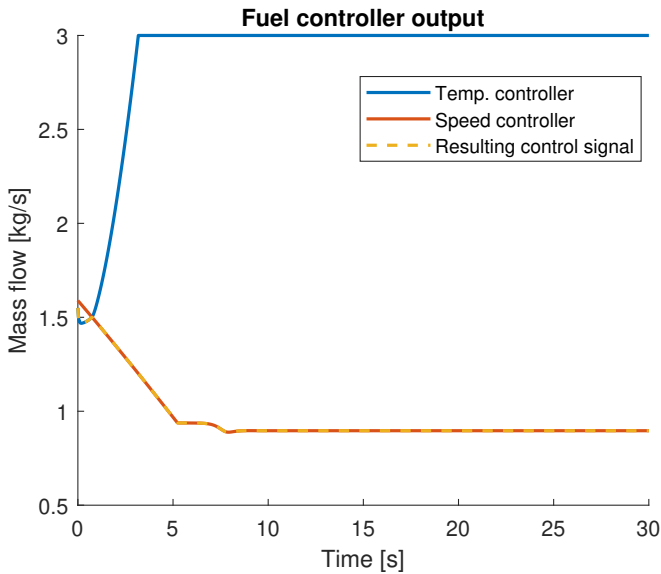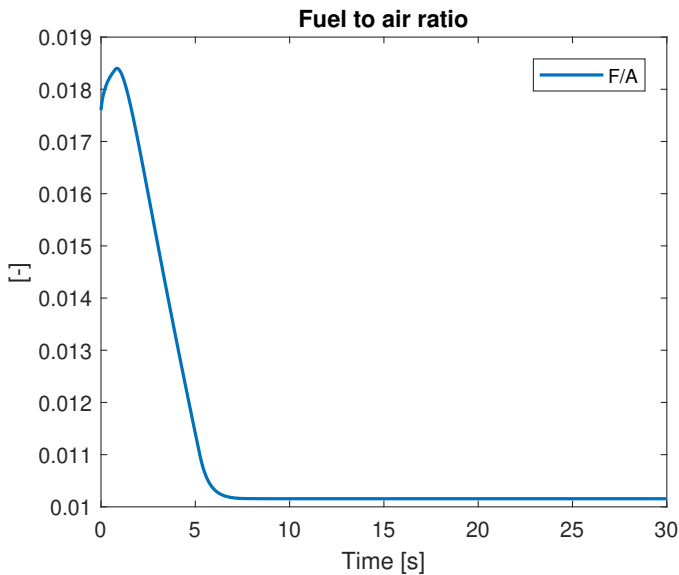
(a) *Torque development during 1000 rpm transient.*
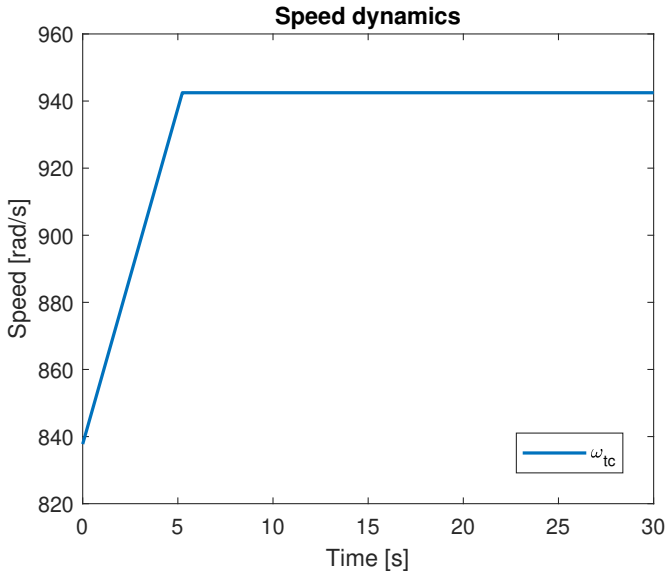
(b) *Speed development during 1000 rpm transient.*

**Figure 4.8:** *Speed and torque development during 1000 rpm transient.*

*(a)* *Fuel controller signals during 1000 rpm transient.*


(b) Fuel to air ratio during 1000 rpm transient.

Figure 4.9: *Fuel mass flow controller signals and fuel to air ratio during the rapid 1000 rpm transient. It can be seen that the speed controller dictates the amount of fuel injected, except during the first moments, where instead the temperature controller produces the smallest control signal.*
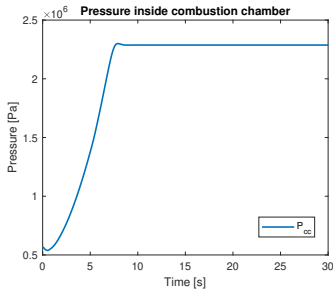
(a) *Combustion chamber pressure.*
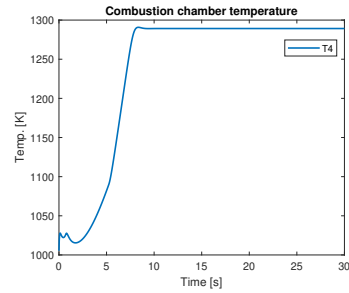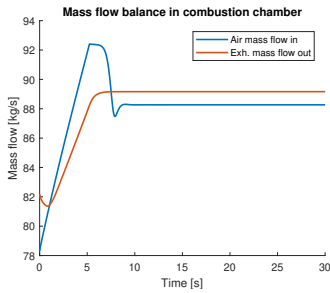
(b) *Combustion chamber temperature.*

(c) *Incoming air mass flow and outgoing exhaust flow.*
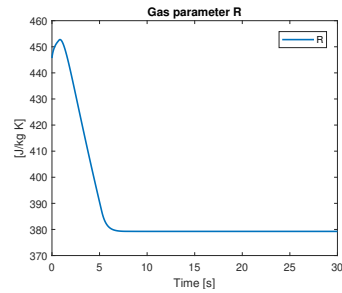
(d) *Specific gas constant R for gas mixture inside combustion chamber.*

Figure 4.10: *Development of various quantities inside the combustion chamber during 1000 rpm transient. Note especially the shifting relation in mass flow in Figure 4.10c.*
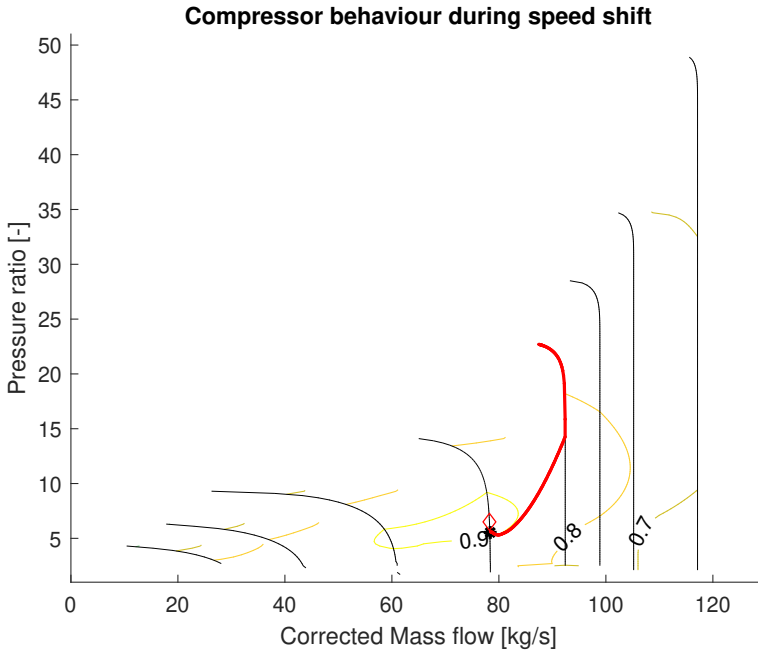
Figure 4.11: *Compressor behavior during 1000 rpm transient. The operation starts off in a good region, as marked by the black spot, but moves along the 9000 rpm speed line and almost into surge.*

the target speed is reached. For evidence of this, compare the pressure development in Figure 4.10a to the speed development in Figure 4.8b, where the pressure keeps rising even after the speed has settled.

When the pressure inside the combustion chamber rises, the pressure ratio across the compressor rises with it. A too large increase in pressure ratio, without an increase in rotational speed will enforce movement almost vertically in the compressor map. When the pressure ratio gets too high, the compressor cannot drive as much air mass flow for a given rotational speed.

Of course, it is of interest to study the transient sequence inside the compressor in further detail. Figure 4.12a, Figure 4.12b and Figure 4.12c shows how stages one, five and nine behave during the transient, respectively. It can be seen clearly that the first stage is the one that is closest to surging. Stage nine moves towards the choke region for a short initially, where the pressure ratio across it (the downstream pressure being the one in the combustion chamber) drops. Stage five in the middle of the compressor pack has a sound behavior but also moves vertically a bit, as the total pressure ratio increase affects it as well.
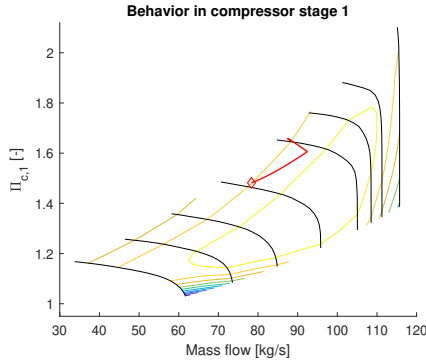
(a) *First stage behavior in terms of flow and pressure ratio.*
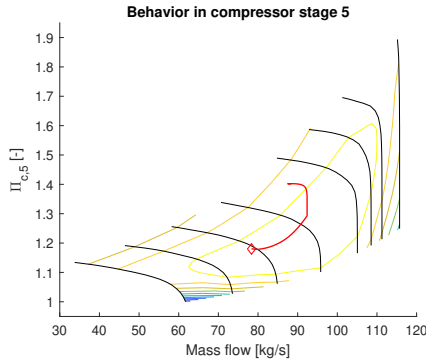
(b) *Fifth stage behavior in terms of flow and pressure ratio.*
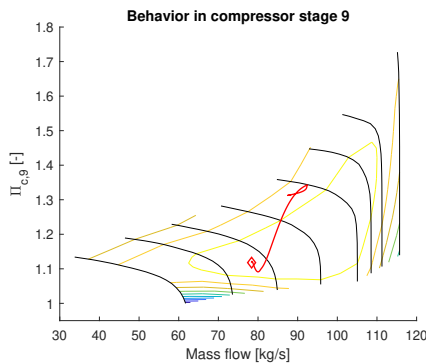
(c) *Ninth stage behavior in terms of flow and pressure ratio.*

Figure 4.12: *Flow and pressure ratio development in stages 1, 5 and 9 during 1000 rpm transient. Red diamond marks starting point. Note that stage 1 drifts towards the surge region, while stage nine drops a little bit towards choke initially, but recovers. Stage 5 operates inside a region of high compressor stage efficiency, which is desirable.*

Model name	Power [MW]	Pressure ratio	Exhaust mass flow [kg/s]	Exhaust temp [°C]	Rated speed [RPM]	Rotor Inertia $[kg \cdot m^2]$
SGT 750 [27]	39.8	24.3	115.4	468	6100	N/A
5001R [1]	19.7	N/A	93	531	4860	626
5001P [1]	25.4	N/A	115	496	4860	919
GE 7F [11]	150	13.5	419	600	3600	N/A
N/A [28]	30.0	23.0	84	N/A	10000	N/A
Model	28	13	82.7	363	10000	1387

Table 4.4: *Comparison of various gas turbine models.*

4.4 Exhaust values

When assessing the gas turbine, it is helpful to compare it to other gas turbines on the market. To investigate whether the scaling of the compressor, turbine, axis and flow components, along with the resulting outputs were reasonable, the simulation output was compared to some of the other gas turbines described in literature and on company web sites. Table 4.4 presents how the gas turbines compare in terms of output power, pressure ratio, exhaust mass flow and exhaust temperature. Since the data comes from various sources, not all information is available for every gas turbine listed. Where data is not available, it is marked with "N/A".

The span of output power in the compared gas turbines ranges from the smaller turbines in the 20 MW region, to the heavy duty General Electric gas turbine of 150 MW. The model in this thesis slots in at an output power of approximately 28 MW. It can be seen that a high pressure ratio does not implicate higher power output. What can be seen is that the model has the highest rated speed and significantly higher inertia than the two where data was available. This seems illogical and should in hindsight be corrected by decreasing the inertia of the model, either by decreasing the mass or radius.

Regarding the exhaust values, it can be seen that the mass flow of 82.7 kg/s is in line with what the other models have listed, except for the significantly larger GE gas turbine. The exhaust temperature of around 360 °C seems to be a bit on the low side, which could be explained by the fact that the fuel mass flow control was a bit conservative and hindered the temperature development.

4.4.1   Stability

The gas turbine model is not very stable. In both flow and power-speed relations, there are a significant amount of parameters that need to combine to stabilize the model, which naturally is very difficult to achieve. During tuning and calibration of the control systems, it became clear that there are some problems regarding the mass flow balance between compressor and turbine, resulting in a tendency to either surge or choke, depending on how the flow parameters are tuned and matched. A clear indication of non-minimum phase behavior is found when studying the pressure ratios during the larger transient in Figure 4.13. The green curve at the bottom of Figure 4.13 is the pressure ratio across stage nine, the last stage, where the combustion chamber pressure is the downstream pressure. It can be seen that it moves downwards initially, but recovers and increases after reaching its minimum, before settling in at steady state. This sort of behavior makes the system very difficult to control, which was very evident during the design of the controllers.
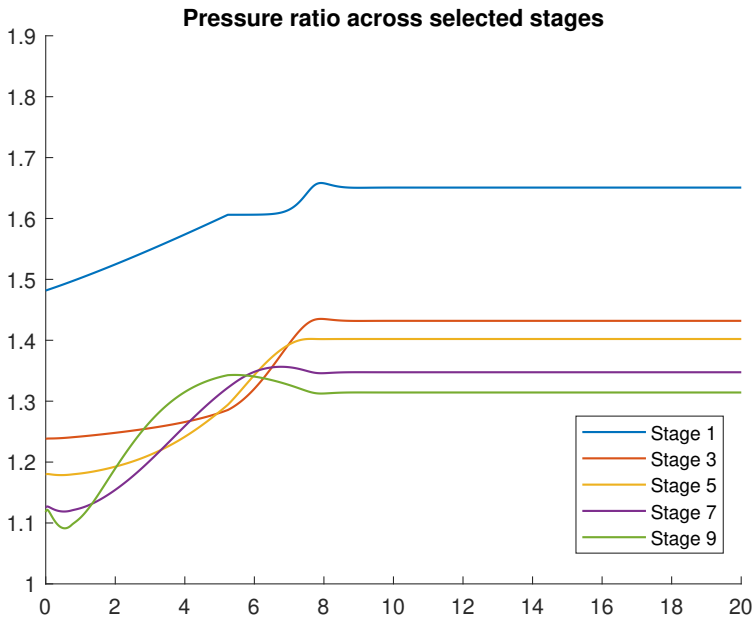

Figure 4.13: *Selected compressor stage pressure ratios during 1000 rpm transient. Note the non-minimum-phase behavior in stage nine (green line).*

The mismatch between incoming and outgoing flow in the combustion chamber leads to either choke or surge, depending on how the turbine map is tuned

and how the fuel injection correlates with that. Since the turbine map is almost flat in terms of flow characteristics at higher speeds - meaning that a shift in pressure ratio impacts the flow minimally - there is a problem in finding a turbine flow that matches the compressor across the significant span of pressure ratios that are present during the simulations. In practice, this means that the model has trouble finding a steady state to settle at.

4.5 Improved controller design

In an attempt to improve the gas turbine performance, particularly in terms of stability margin, a new controller design was developed and implemented. In the original controller design, inspired by Rowen [1], a double PI-controller was used, acting on the rotational speed on one hand, and the turbine exit temperature on the other. This proved to be a functioning design, but it was in no way ideal. Apart from that, the design of the torque/speed control was at best functioning, but there was room for improvement and a bit more creativity there as well.

4.5.1 Controller design

The first problem that materialized when implementing the combined speed and temperature controller, was that the pressure ratio across the last compressor stages presented a non-minimum-phase behavior. It can be clearly seen in Figure 4.13. The pressure ratio drop stems from a lack of fuel injection during the initial phase, leading to a leaner gas composition and temperature, as well as a smaller mass inside the combustion chamber. To mitigate this problem, the new fuel injection controller was designed to operate on the pressure ratio across the ninth stage.

Based on the compressor map for the ninth stage, a pressure ratio curve was created from the optimal pressure ratio for each speed line, in terms of efficiency. The optimal pressure ratio curve can be seen in Figure 4.14. The error signal input to the PI-controller was subsequently the difference between current $\Pi_{c,9}$ and the optimal one.

The other problem that manifested itself in the original model, was that the first stage was prone to surging. It seemed that this problem stemmed from flow imbalances and the fact that the total pressure across the compressor was too high, forcing the first stage into its surge region. Figure 4.20 shows how the first stage starts off closer with a smaller distance to surge, and eventually ends up surging. To counteract this, a controller was designed that operated exactly like the one for the ninth stage. A reference curve was constructed from the optimal pressure ratios for every speed line in the map in terms of highest efficiency, and the difference between current and optimal $\Pi_{c,1}$ was the controller input. The optimal pressure ratio curve for stage nine is show along that of stage one in Figure 4.14.
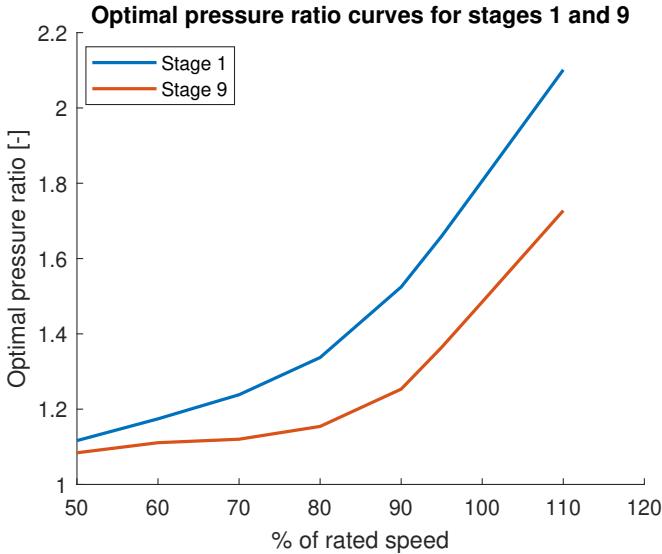
Figure 4.14: *Reference curves for Π_1 and Π_9 controllers.*

An important insight is that the two dangers in the original model manifested themselves in distinctly different phases of the operation - sub-unity pressure ratio across stage nine during the first few seconds, and surge in the first stage at the end of the simulation. Knowing this, the two controllers could be utilized during different phases of the operation, using some form of selector that changes depending on what phase the gas turbine currently is in. The choice of selector was a simple switch based on rotational speed. Switching between two control signals without using a max- or min-selector like in the original design leads to the risk of imposing discontinuities in the control signal, which often is detrimental to performance. However, in this case, it seems to work well. A bit of tuning was made to minimize the difference in control signal values at the switching point at 900 rad/s, in a bid to make the control signal as smooth as possible. Figure 4.15 shows a schematic block diagram of how the improved fuel injection control is designed.

When updating the torque and speed controller, the goal was to make a more reasonable connection between the output net power and the acceleration. The original design was very one-dimensional and mostly designed to facilitate simpler testing of flow matching and fuel injection by isolating it from affecting the speed dynamics. The new design instead correlates the output power to the design power output, meaning that if the net power output is above the design value of 28 MW, it will accelerate the turbine. Conversely, if it is below, it will decelerate it. Figure 4.16 provides a block diagram showing how the controller is designed.
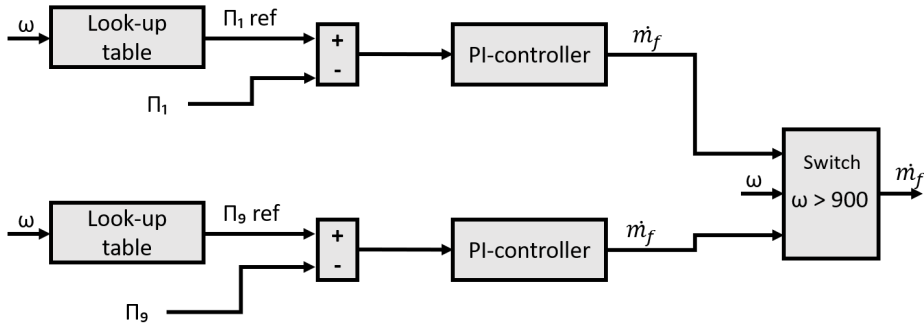
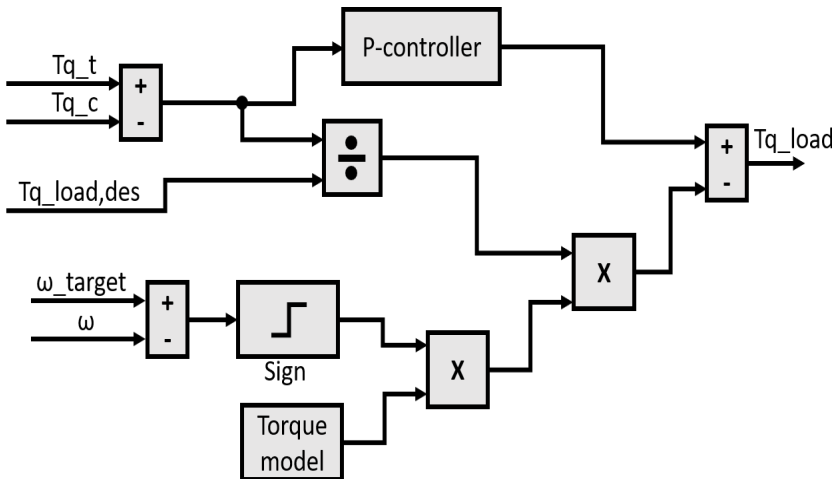**Figure 4.15:** *Updated fuel injection control design.*

Figure 4.16: *Updated torque and speed control design.*

4.5.2   Results using new controllers

When implementing the updated control strategies, the first goal was to obtain a more stable pressure development inside the combustion chamber, and subsequently a less volatile shift in the pressure ratio across the ninth stage in the compressor. This is achieved by basing fuel injection on a quantity more directly related to the combustion chamber pressure. Figure 4.17a shows the new control signals and Figure 4.17b shows the resulting fuel to air ratio during the 1000 rpm transient.

It can be seen that fuel injection initially is quite large, as indicated by both its absolute value and the fuel to air ratio being above the normal guideline value of 0.02. It drastically drops after that, and is in steady decline until the switching

point at approximately 80 seconds, where the fuel injection instead is guided by the pressure ratio across stage one.

Since the pressure ratio across stage one is constantly a bit higher than the reference signal, the control signal from that controller is substantially smaller. The small discontinuity downwards at the switching point at approximately 80 seconds makes the pressure inside the combustion chamber drop, which also affects the pressure ratios across the latter stages in the compressor, which can be seen in Figure 4.19. After the switching point, the fuel flow stabilizes in a gentle slope before reaching the lower saturation imposed in the form of the fuel to air ratio not being allowed to drop below 0.01. Here, the gas turbine as a whole settles at a balanced flow and reaches steady state operation. The control strategies imposed seem to initially provide a quite smooth rise in pressure inside the combustion chamber. Figure 4.18 shows a smooth step with a little drop at the switching point and a more abrupt increase after that.

It is also of interest to study the impact of the control strategies in the individual stages. Figure 4.19 shows how the pressure ratios across stages 1, 3, 5, 7 and 9 develop during the transient. It can be seen that the ninth stage displays a little less volatile fluctuation in pressure ratio and is never in danger of dropping below unity pressure ratio. The non-minimum-phase behavior remains, but is significantly subdued compared to in Figure 4.13. On the other hand does the new control strategy induce a drop in pressure ratio across the rear stages at approximately 80 seconds.

The two objectives of mitigating choking and sub-unity pressure ratio in the rear of the compressor, along with preventing surge in the front is best evaluated by studying the individual stages' compressor maps. Figure 4.20a, Figure 4.20b and Figure 4.20c displays how stages 1, 5 and 9 behave with the new controller design. It can be seen in Figure 4.20a that the first stage still operates in the higher pressure ratio region of the map, but stays well on the right side of the surge line. Figure 4.20b shows that the middle stage holds firmly inside the preferred operating region with high efficiency before the pressure ratio rises and takes it towards lower efficiency. Finally, Figure 4.20c shows that stage nine starts off soundly, drops a bit towards choke, but finds its way into the high efficiency region and then after another drop, it recovers and ends up with a bit on the high pressure ratio side. When studying the compressor map for the entire compressor pack, displayed in Figure 4.21, the differences in performance compared to Figure 4.11 are marginal but clear. The compressor pack follows a similar trajectory with increasing mass flow and pressure ratio, but then makes a little drop before climbing almost vertically in pressure ratio. Finally, it reaches the 9000 rpm speed line and settles with at bit better surge margin than what the initial control strategy provided.
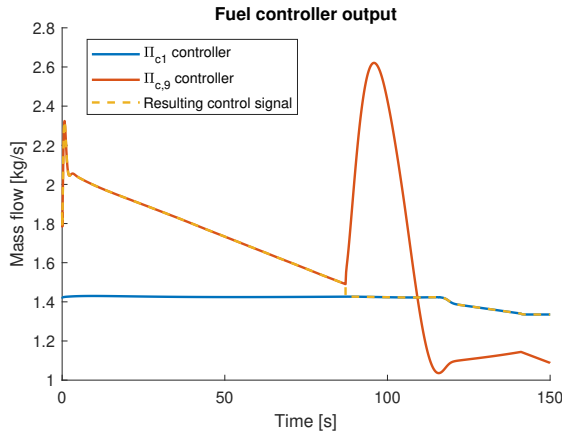
(a) Fuel controller signals during 1000 rpm transient using new controller design. Note the discontinuity at approximately 80 seconds.
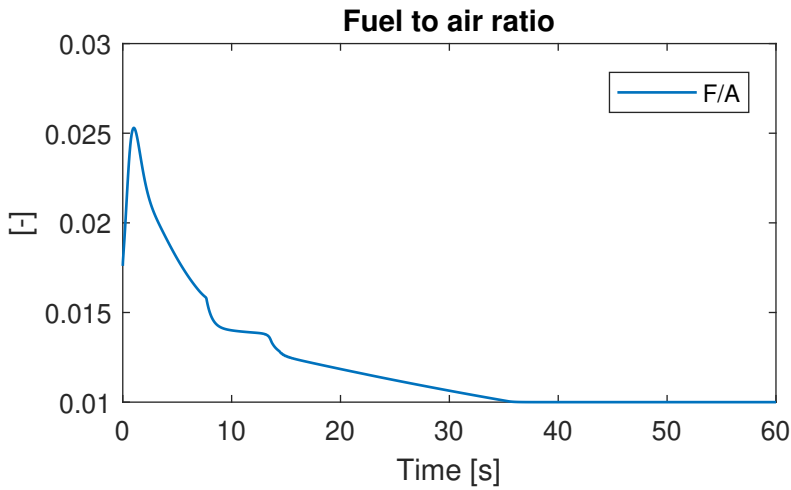
(b) Fuel to air ratio during 1000 rpm transient using new controller design.

Figure 4.17: *Fuel mass flow controller signals and fuel to air ratio during 1000 rpm transient after updating controller design.*
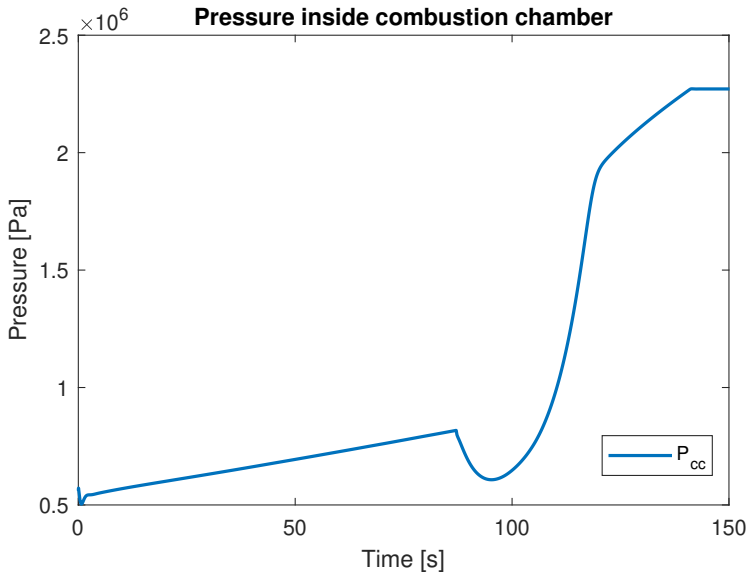
Figure 4.18: *Pressure inside combustion chamber when using updated control design.*

Lastly, the new torque model which allows for a more logical impact of the generated power on the rotational speed, shows that the speed ramping can be performed significantly less urgently. Figure 4.22a shows how the load power varies compared to the design load power of 28 MW. It can be seen that the load power settles at a higher value than the design value.
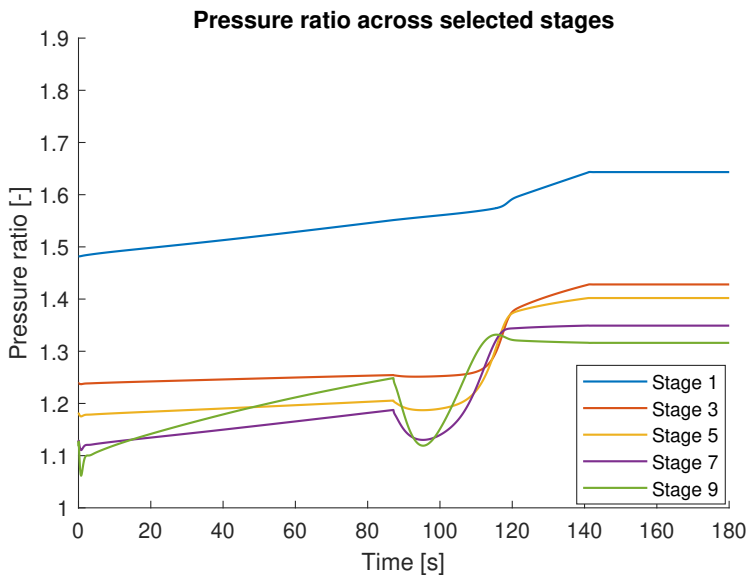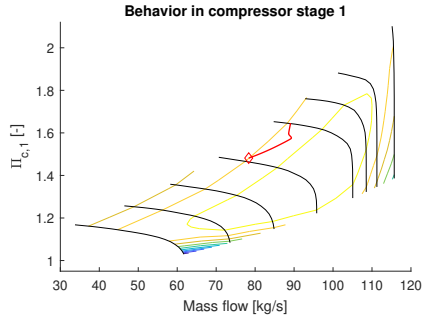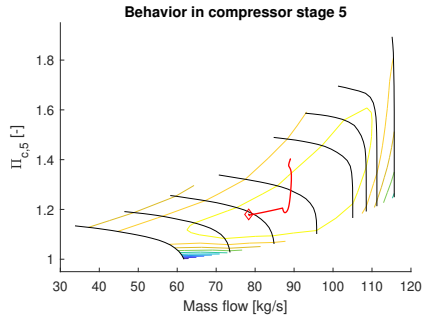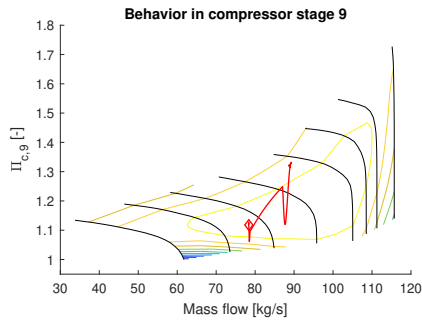
Figure 4.19: *Pressure ratios across compressor stages 1, 3, 5, 7 and 9 when using updated control design during 1000 rpm transient.*

(a) First stage behavior in terms of flow
and pressure ratio.

(b) Fifth stage behavior in terms of flow
and pressure ratio.

(c) Ninth stage behavior in terms of flow
and pressure ratio.

Figure 4.20: Flow and pressure ratio development in stages 1, 5 and 9 during
1000 rpm transient with new controller design. Red diamond marks starting
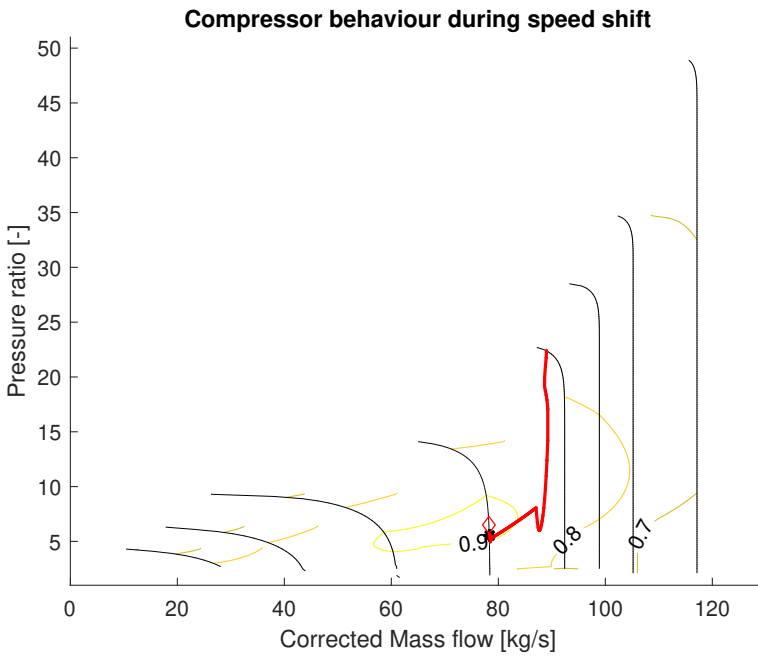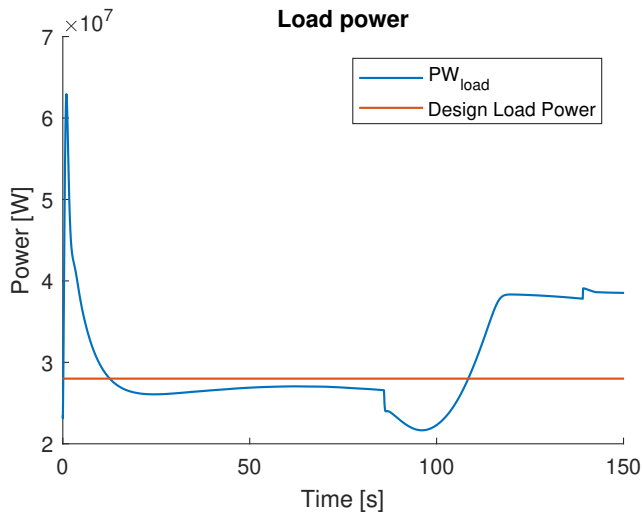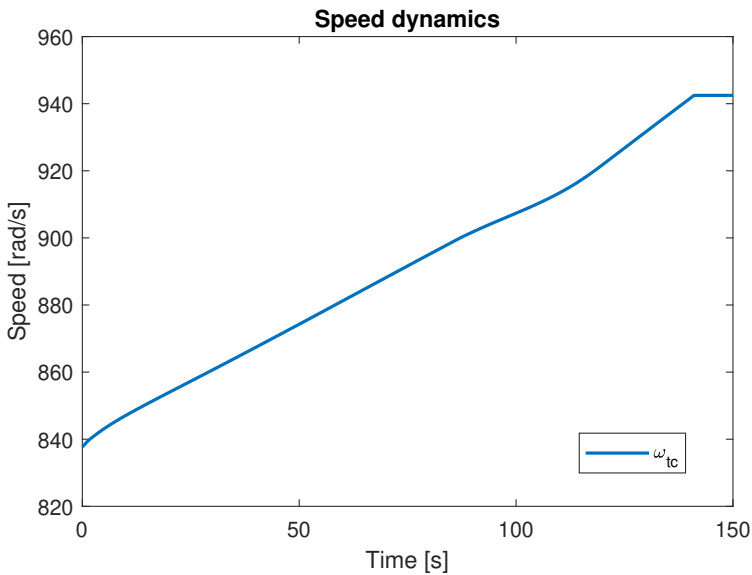point.

Figure 4.21: *Compressor behavior during 1000 rpm transient using new controller design. Red diamond indicates highest efficiency point and black spot shows the starting point.*

(a) *Load power curve during 1000 rpm transient. Red curve is the design point load power, blue curve is the actual load power generated.*

(b) *Speed development during 1000 rpm transient using new load torque design.*

Figure 4.22: *Load power and rotational speed development during 1000 rpm transient after updating controller design. Note that the speed increase is significantly more gentle than when using the initial control strategy.*

5

Conclusions and suggestions for further work

This sections wraps up the conclusions that can be drawn on gas turbine modeling, compressor modeling and the resulting model. The conclusions are gathered in Chapter 5.1 and based on these, some suggestions for further work in the field and extensions of the model are discussed in Chapter 5.2.

5.1 Conclusions

The conclusions that can be drawn based on this thesis can be summarized as follows:

- The modeling of a gas turbine is quite tricky if you are not equipped with actual manufacturer data.

- The Ellipse compressor model works for modeling individual axial compressor stages in a gas turbine.

- Combining stages in series and separating them with control volumes is a feasible way of representing a gas turbine compressor.

- Matching compressor, combustion chamber and turbine in terms of flows, pressures and power output requires a thought-through controlling strategy.

- Separating one big control problem into two smaller ones is sometimes a good approach.

5.2   Further work

Finding a compressor map from a jet engine, scaling it nine different times and
have it represent a multi-stage compressor pack for a gas turbine is a modeling
procedure that probably produces errors. On the other hand, the resulting map
was not that far from a conventional compressor map, so it was not the worst idea,
either. If one was to try to improve this entire GT model, there is little doubt that
the biggest room for improvement lies in the compressor. It would undoubtedly
be interesting to see whether the implementation of some of the more intricate
(and therefore neglected) parts of Kurzke's work on off-design and compressor
scaling would provide a better and more stable model.

Other possible ways to improve the model, would to investigate the impacts
of variable inlet- and outlet guide vanes (VIGV/VOGV). In an actual gas tur-
bine, these are essential parts of the compressor operating reliably during tran-
sients and particularly during start-up. The problem in a MVEM setting, is that
VIGV/VOGV operates on the rotational energy in the air flow, meaning that the
1D-flow model is insufficient. There could quite conceivably be some way of
transferring the VIGV/VOGV angles to changes in pressures and mass flow, thus
allowing simple integration into the MVEM framework from there.

Another possibly intriguing thing to study and integrate into the model, is
limitations to the ignition process and the gas mixture dynamics. Here, the com-
bustion efficiency is considered to be constant, which might be feasible during
steady state operation, but probably is not a very good assumption during start-
up and transients. Furthermore, the gas constants of the exhaust gas is only mod-
eled as a function of the fuel to air ratio, and neglect the temperature impact
completely. A possibly useful extension could be to integrate NASA polynomials
and include the formation of NO_x, which certainly is an important aspect of gas
turbine performance.

The final, and possibly most interesting field of possible further studies, is
the integration of the model into an optimal control framework. This was in the
original scope of the thesis, but proved to be a step too far as the modeling and
simulation was enough of a task on its own. The use of an optimal control tool
would allow for truly fascinating work on how to operate the gas turbine in an
optimal way, and not just "good enough". Since it is well known, and comprehen-
sive underlined in this thesis, that transient behavior in gas turbines is a complex
and intricate business, an optimal control tool equipped with correct limitations
would provide very interesting insight as to how to control the gas turbine in such
situations. Whether it is load shifting, start-up sequences or any other operation
outside steady state, the optimal control framework could - given correct data on
physical limitations and goal functions - provide interesting results. The change
of control strategies in this thesis proved that it was possible to improve perfor-
mance significantly with adequate control strategies based on model knowledge.
To take this a step further, using optimal control, would certainly be interesting.

Bibliography

[1] *Simplified Mathematical Representations of Single Shaft Gas Turbines in Mechanical Drive Service*, volume Volume 5: Manufacturing Materials and Metallurgy; Ceramics; Structures and Dynamics; Controls, Diagnostics and Instrumentation; Education of *Turbo Expo: Power for Land, Sea, and Air*, 06 1992. doi: 10.1115/92-GT-022. URL https://doi.org/10.1115/92-GT-022. V005T15A001.

[2] Hamid Asgari, Mauro Venturini, XiaoQi Chen, and Raazesh Sainudiin. Modeling and simulation of the transient behavior of an industrial power plant. *Journal of Engineering for Gas Turbines and Power*, 2014. doi: 10.1115/1.4026215.

[3] S. M. Camporeale, B. Fortunato, and M. Mastrovito. A Modular Code for Real Time Dynamic Simulation of Gas Turbines in Simulink. *Journal of Engineering for Gas Turbines and Power*, 128(3):506–517, 03 2002. ISSN 0742-4795. doi: 10.1115/1.2132383. URL https://doi.org/10.1115/1.2132383.

[4] Samson Endale Turie. Gas turbine plant modeling for dynamic simulation. Master's thesis, KTH School of Industrial Engineering and Management, Department of Energy Technology, 2011.

[5] Lars Eriksson and Lars Nielsen. *Modeling and Control of Engines and Drivelines*. John Wiley & Sons, 2014.

[6] Lars Eriksson, Lars Nielsen, Jan Brugård, Johan Bergström, Fredrik Pettersson, and Per Andersson. Modeling of a turbocharged si engine. *Annual Reviews in Control*, 26(1):129 – 137, 2002. ISSN 1367-5788. doi: https://doi.org/10.1016/S1367-5788(02)80022-0. URL http://www.sciencedirect.com/science/article/pii/S1367578802800220.

[7] Lars Eriksson, Vaheed Nezhadali, and Conny Andersson. Compressor flow extrapolation and library design for the modelica vehicle propulsion library - vehprolib. In *SAE 2016 World Congress and Exhibition :*, SAE Technical Papers. SAE International, 2016. doi: 10.4271/2016-01-1037.

[8] EM Greitzer. Surge and rotating stall in axial flow compressors—part i:theoretical compression system model. *J. Eng. Power.*, 98(2):190–198, 1976. doi: 10.1115/1.3446138.

[9] EM Greitzer. Surge and rotating stall in axial flow compressors—part ii: Experimental results and comparison with theory. *J. Eng. Power.*, 98(2):199–211, 1976. doi: 10.1115/1.3446139.

[10] JH Kim, TW Song, TS Kim, and ST Ro. Model development and simulation of transient behavior of heavy duty gas turbines. *J. Eng. Gas Turbines Power*, 123(3):589–594, 2001.

[11] JH Kim, TW Song, TS Kim, and Ro ST. Dynamic simulation of full startup procedure of heavy-duty gas turbines. *Journal of Engineering for Gas Turbines and Power*, pages 510–516, 2002. doi: 10.1115/1.1473150.

[12] Koh, Fu Hai Alan and Ng, Yin Kwee Eddie. A one-dimensional stage unstacking approach to reveal flow angles and speeds in a multistage axial compressor at the design operating point. *Mechanics & Industry*, 20(1):107, 2019. doi: 10.1051/meca/2019004. URL https://doi.org/10.1051/meca/2019004.

[13] C. Kong, J. Ki, and M. Kang. A New Scaling Method for Component Maps of Gas Turbine Using System Identification . *Journal of Engineering for Gas Turbines and Power*, 125(4):979–985, 11 2003. ISSN 0742-4795. doi: 10.1115/1.1610014. URL https://doi.org/10.1115/1.1610014.

[14] J Kurzke and C Riegler. A new compressor map scaling procedure for preliminary conceptional design of gas turbines. In *Turbo Expo: Power for Land, Sea, and Air*, volume 1. ASME. doi: 10.1115/2000-GT-0006.

[15] Joachim Kurzke. Correlations hidden in compressor maps. In *ASME 2011 Turbo Expo: Turbine Technical Conference and Exposition*, pages 161–170. Citeseer, 2011.

[16] Emil Larsson. Diagnosis and supervision of industrial gas turbines, 2012. ISSN 0280-7971.

[17] Emil Larsson. *Model Based Diagnosis and Supervision of Industrial Gas Turbines*. PhD thesis, Linköping UniversityLinköping University, Vehicular Systems, The Institute of Technology, 2014.

[18] Oskar Leufvén and Lars Eriksson. Surge and choke capable compressor model. In *Proceedings of the 18th IFAC World Congress, 2011*, pages 10653–10658. International Federation of Automatic Control (IFAC), 2011. ISBN 978-3-902661-93-7. doi: 10.3182/20110828-6-IT-1002.00694.

[19] Oskar Leufvén and Lars Eriksson. A surge and choke capable compressor flow model : Validation and extrapolation capability. *Control Engineering Practice*, 21(12):1871–1883, 2013. doi: 10.1016/j.conengprac.2013.07.005.

[20] Xavier Llamas and Lars Eriksson. Parameterizing compact and extensible compressor models using orthogonal distance minimization. *Journal of engineering for gas turbines and power*, 139(1):GTP-15-1569, 2017. doi: 10.1115/1.4034152. Funding Agencies|European Union [634135].

[21] Xavier Llamas and Lars Eriksson. Control-oriented compressor model with adiabatic efficiency extrapolation. *SAE International Journal of Engines*, 10 (4), 2017. doi: 10.4271/2017-01-1032.

[22] Paul Moraal and Ilya Kolmanovsky. Turbocharger modeling for automotive control applications. In *International Congress & Exposition*. SAE International, mar 1999. doi: https://doi.org/10.4271/1999-01-0908. URL https://doi.org/10.4271/1999-01-0908.

[23] Seik Park, Gyung Min Choi, and Mamoru Tanahashi. Demonstration of a gas turbine combustion-tuning method and sensitivity analysis of the combustion-tuning parameters with regard to nox emissions. *Fuel*, 239: 1134 – 1142, 2019. ISSN 0016-2361. doi: https://doi.org/10.1016/j. fuel.2018.11.021. URL http://www.sciencedirect.com/science/ article/pii/S0016236118319057.

[24] V.C. Patel, V. Kadirkamanathan, H.A. Thompson, and P.J. Fleming. Utilising a simulink gas turbine engine model for fault diagnosis. *IFAC Proceedings Volumes*, 28(26):237 – 242, 1995. ISSN 1474-6670. doi: https://doi.org/ 10.1016/S1474-6670(17)44764-1. URL http://www.sciencedirect. com/science/article/pii/S1474667017447641. IFAC Symposium on Control of Power Plants and Power Systems 1995, Cancún, Mexico, 6-8 December.

[25] ER Rademaker. Scaling of compressor and turbine maps on basis of equal flow mach numbers and static flow parameters. 2012.

[26] Manoj R Rajanna, Fei Xu, Ming-Chen Hsu, Yuri Bazilevs, Muthuvel Murugan, Anindya Ghoshal, and Luis G Bravo. Optimizing gas-turbine operation using finite-element cfd modeling. In *2018 Joint Propulsion Conference*, page 4657, 2018.

[27] Siemens. Sgt-750 fact sheet, 2016. URL https:// assets.new.siemens.com/siemens/assets/api/uuid: 35fea654a25de98622791f45a6652c6e3b12441b/version: 1528903230/sgt-750-factsheet-en.pdf.

[28] E Tsoutsanis, N Meskin, M Benammar, and K. Khorasani. Dynamic performance simulation of an aeroderivative gas turbine using the matlab simulink environment. *ASME International Mechanical Engineering Congress and Exposition, Volume 4A: Dynamics, Vibration and Control*. doi: 10.1115/IMECE2013-64102.

[29] Philip P. Walsh and Paul Fletcher. *Gas Turbine Performance*. Blackwell Science, second edition, 2004.

[30] Qingcai Yang, Shuying Li, and Yunpeng Cao. A new component map generation method for gas turbine adaptation performance simulation. *Journal of Mechanical Science and Technology*, 31(4):1947–1957, Apr 2017. ISSN 1976-3824. doi: 10.1007/s12206-017-0344-5. URL https://doi.org/10.1007/s12206-017-0344-5.

[31] Luis J Yebra, Sebastian Dormido, Luis E Diez, Alberto R Rocha, Lucia Gonzalez, Eduardo Cerrajero, and Silvia Padilla. Object-oriented dynamic modelling of gas turbines for csp hybridisation. pages 926–933, 12 2018. doi: 10.3384/ecp17142926.